Sensor Fusion for Navigation of Autonomous Underwater Vehicle using Kalman Filtering

Akash Agarwal

Department of Electrical Engineering
National Institute of Technology Rourkela
2010-2015

Sensor Fusion for Navigation of Autonomous Underwater Vehicle using Kalman Filtering

A thesis submitted in partial fulfillment of the
requirements for the award of the degree of

Bachelor of Technology and
Master of Technology Dual Degree

in

Electrical Engineering

by

Akash Agarwal
Roll - 710EE3123

Under the Guidance of

Prof. Bidyadhar Subudhi

Department of Electrical Engineering
National Institute of Technology Rourkela
2010-2015

Department of Electrical Engineering

National Institute of Technology, Rourkela

CERTIFICATE

*This is to certify that the thesis entitled "**Sensor Fusion for Navigation of Autonomous Underwater Vehicle using Kalman Filtering**" by **Mr. Akash Agarwal**, submitted to the Department of Electrical Engineering, National Institute of Technology, Rourkela, India, during the academic session 2010-2015 for the award of Bachelor of Technology and Master of Technology Dual Degree in Electrical Engineering, is a record of bona fide research work carried out by him under my supervision and guidance. The thesis has fulfilled all the requirements as per the regulations of this institute and in my opinion has reached the standard for submission.*

Prof. Bidyadhar Subudhi

Department of Electrical Engineering,

NIT Rourkela, India

Place: Rourkela, India

Date:

Acknowledgement

First and foremost, I am truly indebted to my supervisor Prof. Bidyadhar Subudhi for his inspiration, guidance and unwavering confidence throughout my study, without whom this thesis would not be in its present form. I also thank him for his gracious encouragement throughout the work.

I am also very much obliged to the Head of the Department of Electrical Engineering, NIT Rourkela for providing all the possible facilities towards this work. I express my warm gratitude to all the professors of Department of Electrical Engineering for helping me with the courses of Electrical Engineering that was instrumental for completing this thesis.

I would like to extend my special gratitude to my friends Aman, Vishnu, Sharda and Ashish, without whom, this journey would not have been this enjoyable.

My wholehearted gratitude to my beloved parents for their encouragement, inspiration and support.

Akash Agarwal

Abstract

An Autonomous Underwater Vehicle (AUV) is a robot that can travel underwater without requiring any intervention from the operator. As opposed to AUV, Remotely Operated Vehicle (ROV) is an underwater robot which requires manual control through a tethered wire connected to a base ship or a station. AUV finds tremendous applications in the field of defense, underwater mine detection, study of ocean floor, repair of undersea cables and is also pursued as a hobby. For an automated vehicle to travel from point A to point B, requires three interrelated technologies: Navigation, Guidance and Control. This thesis mainly focuses on the Navigation aspect of the AUV.

Inertial Navigation System (INS) use accelerometers and gyroscopes to measure acceleration and attitude (orientation) rates respectively to estimate position, velocity and attitude in three orthogonal directions. Global Navigation Satellite System (GNSS) uses a cluster of satellites to estimate the position of GNSS receiver close to the surface of the earth. INS gives accurate short term navigation solutions yet its accuracy diminishes over the long run because of accumulation of errors. The precision of GNSS navigation solution is not so good when contrasted with INS but they don't corrupt over the long run. When these two navigation systems are fused or integrated using a Kalman filter, the subsequent system performs better than either of the individual systems even when sensors of lower cost and lower performance are used. One disadvantage of using GNSS is that the GNSS signals are lost whenever the AUV dives inside the water. But by using an integrated GNSS/INS system, an INS is allowed to navigate with improved initial error even when GNSS signals are lost, thus achieving the desired standalone performance. Moreover, whenever the GNSS signals are available, the system utilizes the INS data to decrease the signal reacquisition time for GNSS. Thus each system supports the other system to achieve the desired performance.

The thesis focuses on the design and implementation of Kalman filters for these applications. First of all, dynamic model and sensor error model for strapdown INS has been developed. The effectiveness of the model was studied using Schuler oscillation test, bias error test and stationary INS test. Next, an error model for GNSS has been developed. Subsequently, various

types of vehicle dynamic model for GNSS receivers has been developed and its error characteristics were compared using a simulated Figure-8 track (track in the shape of 8). Finally, performance analysis of INS, GNSS and integrated GNSS/INS is studied on a Figure-8 simulated track. Effect of loss of GNSS signals on the performance is also studied.

Contents

List of Abbreviations

Abbreviation	Description
INS	Inertial Navigation System
GNSS	Global Navigation Satellite System
GPS	Global Positioning System
GLONASS	Global Orbiting Navigation Satellite System
STF	Signal Task Force
PRC	People's Republic of China
AUV	Autonomous Underwater Vehicle
ROV	Remotely Operated Vehicle
MEMS	Micro-Electro-Mechanical Systems
ECI	Earth-Centered Inertial
ECEF	Earth-Centered, Earth Fixed
LTP	Local Tangent Plane
RPY	Roll-Pitch-Yaw
ENU	East-North-Up
NED	North-East-Down
ISA	Inertial Sensor Assembly
IMU	Inertial Measurement Unit
HVAC	Heating, Ventilating and Air Conditioning
RMS	Root Mean Square
MSB	Most Significant Bit
DOP	Dilution of Precision
GDOP	Geometric Degree of Precision
PDOP	Position Degree of Precision
HDOP	Horizontal Degree of Precision
VDOP	Vertical Degree of Precision
TDOP	Time Degree of Precision
CEP	Circle of Equal Probability
DVL	Doppler Velocity Log

List of Figures

List of Tables

Chapter 1

Introduction

1.1. Background

The theoretical foundation of INS have been known since the time of Newton but the technology was inadequate for practical implementations due to inaccurate sensors, incompatible methods for integrating the sensor outputs and inadequate software available. The inertial navigation was largely developed during the Cold War between the Soviet Union and the United States. Nuclear weapons were available with both sides but neither had compatible long range delivery systems. During this time, Charles Stark Draper who is known as the Father of Inertial Navigation demonstrated a first successful inertial navigation performance aboard a Boeing B-29 bomber on a flight from Bedford to Los Angeles. Since then, INS has undergone massive improvements. GNSS was also a result of navigation solution requirement during Cold War. NAVSTAR GPS was the first successful implementation of GNSS which was put into operation in 1980's by the U.S. Department of Defense. By the time Cold War ended, both GPS and INS technology matured considerably, not only in terms of accuracy but also in terms of cost and weight. Now, the cost of GNSS/INS systems have lowered to a point that it can be embedded in consumer products.

1.2. Navigation

The word navigation was derived from the Latin word '*navis*' (ship) and '*agare*' (drive) to designate the operation of a ship on a voyage. For a vehicle to move from point A to point B, some kind of observation is required to determine one's present location relative to the final destination. There are five types of navigation that are used:

- Pilotage: It relies on external landmarks such as mountains and seas to know its position. It is obsolete and no longer used.
- Celestial Navigation: It was inspired from birds who could use celestial objects to navigate from one place to another. Celestial Navigation uses time and the angle

between local vertical and celestial objects such as sun, moon and stars to estimate longitude, latitude and orientation.

- Dead reckoning: It uses initial position, plus magnetic compass (to know the heading information) and some estimate of speed to determine the distance travelled and the position of the vehicle.
- Radio Navigation: It relies on radio-frequency sources such as beacons in satellites, receiver and transmitter technology to estimate position of the object. GNSS is a form of radio navigation and the clocks used in these satellites should be highly accurate to give an accurate estimate of the position of the receiver.
- Inertial Navigation: It is an upgraded version of the dead reckoning system. It takes initial values of position, velocity and orientation and then measures accelerations and attitude rates using accelerometer and gyroscope respectively to estimate position, velocity and orientation. As, this form of navigation does not rely on external sources, it is the most reliable form of navigation used for military purposes.

This thesis focuses on the integration of the last two types of navigation i.e. Radio Navigation and Inertial Navigation using a Kalman filter. When these two navigation systems are fused, the resulting system performs better than either of the individual systems even if sensors of lower cost and lower performance are utilized.

For an automated vehicle to travel from one point to another, requires three interrelated technologies: Navigation, Guidance and Control.

- Navigation: It refers to the art of estimating the current position, velocity and attitude of a vehicle using INS, GNSS or other navigation methods. The vehicle could be in space, in air, on land, on the surface of water or under the surface of water. The sensors data are usually corrupted by noise and sometimes the measurements are unavailable. In such cases, the noise must be filtered out and the missing state should be estimated. An accurate estimation of vehicle position and attitude is vital as the errors may affect the functioning of guidance and control systems of the vehicle.
- Guidance: It refers to the art of determining an optimum path of a vehicle given the initial and final state. The states may include position, velocity, attitude or attitude rates. The constraints may involve factors such as time, cost, fuel, risks, etc.

- Control: It refers to the art of determining required forces and torques for getting the vehicle to follow a desired path or trajectory. Different objectives which can be addressed by the control structure are trajectory tracking, path following and way point tracking.

The distinctions between these three technologies may be blurred but it could be better understood with the help of an example. Consider a GPS system installed in a highway car. Navigation gives the driver an initial position estimate of the vehicle on the map as well as position estimate as the car moves through the highway. Guidance finds an optimum route from starting point A to the destination B considering time and distance as constraints. Control refers to the actions taken by the driver to follow the planned route.

The thesis largely focuses on the navigation aspect of AUV using the integration of INS and GNSS.

1.3. Kalman Filter in Navigation

Kalman Filter is often referred as “navigation ‘s integration workhouse”. Kalman filter in navigation was first successfully implemented in the Apollo mission to estimate the trajectory of the spacecraft from the earth to the moon. Without Kalman Filtering, it would have been extremely unlikely that the mission would have succeeded. Apart from estimating position, Kalman filter produces an estimate of its own accuracy because of which it has form an integral part in the design and implementations of navigation solutions and sensor integration. GNSS and INS systems have complementary (enhancing each other) error characteristics and Kalman Filter takes advantage of these characteristics to enhance the performance of either of the system. Kalman Filter is defined completely by φ, Q, H and R and to some extent on P as well. The statistical and dynamical information about the errors of both INS and GNSS has to be studied to completely design the Kalman Filter.

In this work, Kalman Filter would be used to develop and implement following models:

- Dynamic model of the host vehicle which is to be tracked
- Sensor error characteristics of INS
- Error and statistical characteristics of GNSS receiver
- Processing of pseudorange measurements
- Integrated GNSS/INS navigation systems model

1.4. Motivations

Navigation forms an important aspect of the AUV structure. The errors introduced in the navigation phase can also transform into control instability. INS and GNSS are the major systems that are used in navigation. INS gives accurate short term navigation solutions but its accuracy deteriorates over time due to accumulated of errors. The accuracy of GNSS navigation solutions is not so good as compared to INS but they do not degrade over time. By exploiting the statistical characteristics of these two systems, Kalman Filter is able to consolidate a system with several meters of position uncertainty (GNSS) with another system whose position uncertainty deteriorates at the rate of kilometers per hour (INS) and attain a bounded position uncertainty of the order of centimeters and meters. Due to increase in accuracy of the overall system, sensors and receivers of lower cost and poor performance can also be used, thus decreasing the overall cost. Another advantage of using an integrated GNSS/INS system is that an INS is allowed to navigate with improved initial error even when GNSS signals are lost, thus achieving the desired standalone performance. Moreover, whenever the GNSS signals are available, the system utilizes the INS data to decrease the signal reacquisition time for GNSS. Thus each system complements the other system to achieve the desired performance.

1.5. Objectives of the Thesis

The objectives of the thesis are as follows:

- To develop an INS model for navigation error dynamics and sensor error dynamics and test the validity of model by performing Schuler oscillations test.
- To develop an error model for GNSS and study the effect of these models on a simulated Figure-8 track and also study the effect of satellite geometry on positioning.
- To track the drifting parameters of the INS sensors, so that INS performance does not degrade with time when GNSS is available.
- To allow the INS to navigate with improved initial error whenever the GNSS signals are unavailable.
- To help improve signal reacquisition and reduce signal phase tracking lags in the GNSS receiver by using the INS data whenever the GNSS signals becomes available again.

1.6. Thesis Organization

The thesis is organized as follows,

- Chapter 2 presents a literature survey on the various systems used in GNSS and INS integration. The unique contributions of different publications in this field are reviewed and acknowledged.
- Chapter 3 presents the different types of coordinate systems that needs to be studied to arrive at a common navigation solution. The transformation algorithm from one reference frame to another is also explained.
- Chapter 4 starts with the basics of INS and describes the various operations that are needed to estimate position and attitude. The navigation error models and sensor error models has been developed. Various analysis is done on the model to study INS performance.
- Chapter 5 provides an introduction to GNSS satellite structure and signal characteristics. Various terms associated with GNSS and various phenomenon such as dilution of precision and dilution of information has been explained. GNSS error models were tested in ‘figure 8’ track using host vehicle dynamics.
- Chapter 6 presents a unified model to be used in GNSS and INS integration and various performance analysis on the model was also done.
- Chapter 7 concludes the thesis and scope of future work are also discussed.

Chapter 2

Literature Review

1960's is regarded as the Space Age. During this time, Kalman filter with its application in inertial navigation found its first use in the Apollo mission. Since then many developments has been made in the inertial navigation system and are now used in many military and commercial applications. This was the result of simultaneous development of theory, components and subsystems of INS. In [1], many of the historical happenings in the development of INS has been accounted. Kalman Filter was first introduced in 1960 and since then, it became an integral part of navigation systems. Because of the simplicity of the algorithm, Kalman filter is particularly useful for conveniently integrating (or fusing) navigation sensor data to achieve optimal system performance. Apart from providing current estimates of the system parameters, the filter can also determine up-to-date uncertainties of the estimates. Because of the ease of implementation and optimum performance, the Kalman filter is often regarded as the 'Navigation's Integration Workhorse'. [2] introduces us to Kalman filtering applications and how it could be applied to GPS/INS integration.

Reference [3] deals with the theoretical and practical aspects of Kalman filtering. It provides several practical aspects of implementation in real world environments such as modelling of the problem, analyzing the performance of the estimator, implementation of stable algorithms and ways to test the results. Some basic understanding of INS and GNSS systems and how Kalman filter is used for their integration has also been provided in [3]. Navigation using different navigation systems needs to be solved in their respective coordinate frame: inertial coordinates frame for INS, satellite coordinate frame for GNSS and Local Tangent Plane (LTP) for representing coordinates on the surface of earth. Reference [4, 10] provides an overview of different navigation reference coordinate system and the transformations that are needed to transform a vector from one frame to another. Reference [10] also deals with the kinematics, dynamics and the equations of motion for an AUV robot.

There are two types of INSs available: Gimbaled and Strapdown. Gimbaled INS use gimbal rings to isolate sensors from the rotation of vehicle. This provides mechanical isolation from shocks and vibration. Strapdown INSs are microelectromechanical systems (MEMS) and they use software to replace gimbals. Due to vibration modes, coning and skulling motion is introduced and this creates a problem for attitude integration in Strapdown INS. John Bortz developed a model for attitude integration based on measured rotation rates and rotation vectors and is discussed in [11].

There are various types of sensors errors introduced in the INS at the time of measurement of sensor inputs such as scale factor errors, sensor biases and misalignments. These errors must be compensated and the original sensor inputs must be recovered. This process is called sensor compensation and is discussed in [12]. [12] also uses Kalman filtering to compensate for drifting sensor errors by integrating INS with GNSS. [8] provides a clear and concise description of the principles of the Strapdown inertial navigation system. It discusses about the different types of accelerometers and gyroscopes and an elaborate note on MEMS technology has also been provided. The methods and techniques are explained with the help of a design example, which includes illustrations for defining and analyzing the problem and designing an appropriate solution. [8] also provides some novel techniques to sense angular and linear motion. The navigation error models and sensor error models for INS has been dealt in detail in [6].

[5] deals with more of practical implementation of GNSS, INS and GNSS/INS integration. It includes Kalman filter models and methods required for GNSS/INS integration. It also gives a detailed description of the GNSS technology with Matlab examples. Formulation of mathematical model of a problem, analyzing performance, assessing the computational requirement and testing the validity of the results are some other practical aspects of implementation that are dealt with in [5].

[9] presents a detailed fundamental information on Global Positioning System (GPS) receivers. Signal characteristics of a GPS signal and how to extract useful information from it has also been presented. Software examples to track GPS signals are provided to give a better understanding on the working of GPS receivers. In addition, a detailed description of satellite constellation and Earth Centered, Earth-Fixed (ECEF) Coordinate system has been provided.

Chapter 3

Coordinate Systems and Transformations

3.1. Introduction

Navigation using different navigation systems needs to be solved in their respective coordinate frame: inertial coordinates frame for INS, satellite coordinate frame for GNSS and Local Tangent Plane (LTP) for representing coordinates on the surface of earth. The major coordinate system used and the transformation between them is explained in this chapter. The transformation between one coordinate system to other is often represented by orthogonal matrices. However, the transformation can also be represented by Euler Angles, Quaternions, Rotation vectors and others. This chapter provides the basic concepts required to understand the solution of the navigation problem.

3.2. Coordinate Transformation Matrix

We will use the notation $\mathbf{C}_{\mathrm{TO}}^{\mathrm{FROM}}$ to signify a coordinate transformation matrix from one coordinate frame ("FROM") to another coordinate frame ("TO"). For example, the matrix $\mathbf{C}_{\mathrm{RPY}}^{\mathrm{ENU}}$ indicates the transformation from East-North-Up (ENU) coordinate frame to Roll-Pitch-Yaw (RPY) coordinate frame.

As a general case, suppose a vector $\mathbf{v}$ in XYZ coordinates is represented as

$$\mathbf{v} = \begin{bmatrix} v_x \\ v_y \\ v_z \end{bmatrix} \tag{3.1}$$

and the same vector $\mathbf{v}$ in UVW coordinates is represented as

$$\mathbf{v} = \begin{bmatrix} v_u \\ v_v \\ v_w \end{bmatrix} \tag{3.2}$$

then, the transformation represented by

$$\begin{bmatrix} v_x \\ v_y \\ v_z \end{bmatrix} = \mathbf{C}_{\mathrm{XYZ}}^{\mathrm{UVW}} \begin{bmatrix} v_u \\ v_v \\ v_w \end{bmatrix} \tag{3.3}$$

will transform the coordinates from UVW coordinates to XYZ coordinates.

3.2.1. Properties of Coordinate Transformation Matrix

- Composition Rule:

$$\mathbf{C}_{\mathrm{C}}^{\mathrm{B}}\mathbf{C}_{\mathrm{B}}^{\mathrm{A}} = \mathbf{C}_{\mathrm{C}}^{\mathrm{A}} \tag{3.4}$$

- Orthogonality:

$$\left(\mathbf{C}_{\mathrm{B}}^{\mathrm{A}}\right)^{T} = \mathbf{C}_{\mathrm{A}}^{\mathrm{B}} \tag{3.5}$$

Note:

- The origin of the coordinate system before and after the transformation remains the same.
- In case there is an origin shift from one frame to another, equation (3.3) gets modified as:

$$X_{XYZ} = \mathbf{C}_{\mathrm{XYZ}}^{\mathrm{UVW}} X_{UVW} + S_{XYZ} \tag{3.6}$$

  where S_{XYZ} is the coordinate origin shift vector in XYZ coordinates.
  However, if X_{UVW} is a unit vector in the UVW coordinate frame, the transformed X_{XYZ} vector will also be a unit vector in the XYZ coordinate frame and hence there is no need of origin shift.

3.3. Coordinate Systems

The coordinate systems are application specific. For INS/GNSS integration, these are the major coordinates system that would be used:

I. Inertial Coordinates:
   a) Earth-Centered Inertial (ECI)
   b) Satellite Orbital Coordinates

II. Earth fixed Coordinates:
   a) Earth-Centered, Earth Fixed (ECEF)
   b) Local Tangent Plane (LTP)

III. Vehicle fixed Coordinates:
   a) Roll-Pitch-Yaw (RPY)

Study of these coordinates system and transformations between them is important for understanding the model of INS and GNSS as well as INS/GNSS integration.

3.3.1. ECI Coordinates

The ECI coordinates are the inertial coordinates in the near earth environment. The origin is at the center of the earth and the orthogonal axis directions as,

x, in the direction of vernal equinox

z, along the north polar axis

y, an axis defined to form a right-handed orthogonal coordinate system

Equinoxes are the time when the sun is directly over the Equator and it happens twice a year. **Vernal Equinox** is one of those equinoxes that occurs when the sun appears to be moving from Southern hemisphere to Northern hemisphere over the equatorial plane. The direction to the sun from the earth at the time of Vernal Equinox is defined as the x direction for ECI coordinates as shown in Figure 3.1.

The equatorial plane of ECI coordinates coincides with the equatorial plane of earth but the earth itself is rotating relative to the ECI coordinate frame at the rate of 15.04109 deg/h.

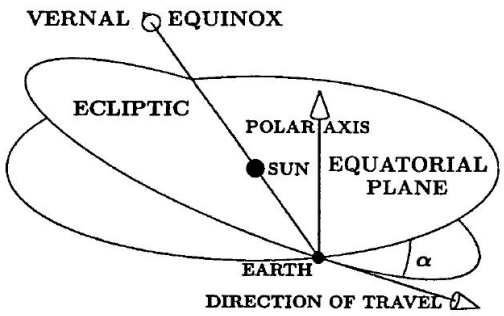

Fig 3.1: Direction of Vernal Equinox [4]

3.3.2. Earth-Centered, Earth-Fixed (ECEF) Coordinates

ECEF coordinates have the same origin and polar axis as of ECI coordinates, but the x axis of ECI coordinate rotates with the Prime Meridian (Greenwich) longitude of the earth as shown in Figure 3.2. Hence, ECI and ECEF coordinates differ only by a function of time. Longitudes and Latitudes are defined in ECEF coordinates. Longitudes are measured east(+) and west(-) with respect to the prime meridian. The angle between the pole star and the local gravitational vertical direction is approximated as geodetic latitude.

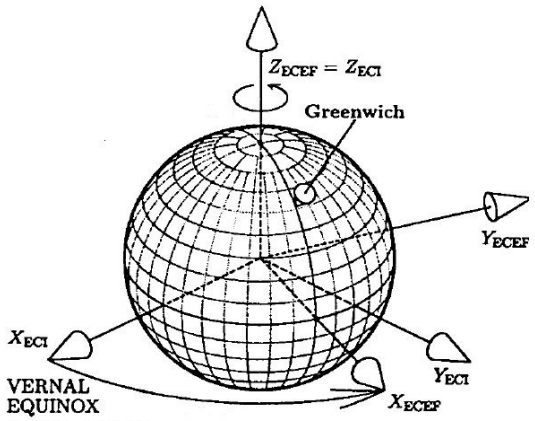

Fig 3.2: ECI and ECEF coordinates [4]

3.3.3. Satellite Orbit Coordinates

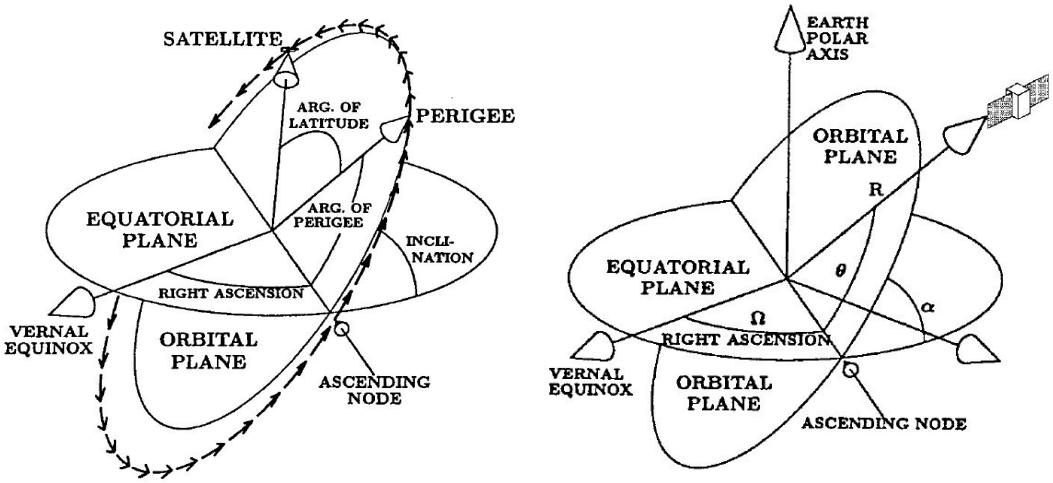

Fig 3.3: Satellite Coordinates [4]

Johannes Kepler characterized the base number of parameters needed to determine an orbit called as "Keplerian" parameters as shown in Figure 3.3 and are defined as follows:

- Right ascension of ascending node (Ω_0) is measured in counter clockwise direction from vernal equinox as seen looking down from north polar axis. The line of intersection of equatorial plane and the orbital plane is known as the 'line of nodes' where the nodes are the two intersection points of the satellite orbit with the line. The two nodes are termed as ascending or descending depending on the satellite path.
- Orbital inclination (α) is the acute angle between equatorial plane and orbital plane. It ranges between $0^0$to 90^0.

- Argument of Perigee: Perigee is the point when the satellite is closest to the earth. The angle between the perigee and the ascending node is termed as Argument of Perigee.
- "Argument of latitude" or "true anomaly" is the angle of the satellite with respect to the perigee of the elliptical orbit.
- Semimajor axis a and semiminor axis b defines the shape and size of the elliptical orbit within the orbital plane.

For computer simulation purpose, it is assumed that the GNSS satellite coordinates are circular i.e. a = b = R = 26,560 km and α as 55°.

The nominal satellite position in Earth Centered Earth Fixed (ECEF) coordinates is then given as,

$$x = R[\cos\theta\cos\Omega - \sin\theta\sin\Omega\cos\alpha] \quad (3.7)$$

$$y = R[\cos\theta\cos\Omega + \sin\theta\sin\Omega\cos\alpha] \quad (3.8)$$

$$z = R\sin\theta\sin\alpha \quad (3.9)$$

$$\theta = \theta_0 + (t - t_0)\frac{360}{43{,}082}deg \quad (3.10)$$

$$\Omega = \Omega_0 + (t - t_0)\frac{360}{86{,}164}deg \quad (3.11)$$

$$R = 26{,}560{,}000\ m \quad (3.12)$$

Where,

R is the radius of the satellite orbit

x, y, z are the satellite coordinates in ECEF coordinate frame

Ω_0 is the Right ascension of ascending node at time $t = t_0$

θ_0 is the angular phase of satellite within the orbital plane at time $t = t_0$

3.3.4. Local Tangent Plane (LTP) Coordinates

LTP coordinates are defined on or near the surface of the earth with the origin of LTP coordinates as a point on the surface of the earth. The point is a particular latitude and longitude on the surface of the earth. LTP coordinates represents the earth as being locally flat as shown in Figure 3.4. These coordinates are especially useful from a human point of view for representing local coordinates and attitudes of host vehicle. The horizontal axis of

the LTP coordinates is along the increasing latitude and is called as the north axis. The other horizontal axis is along the direction of increasing longitude and is called as the east axis. The coordinate system is as shown in Figure 3.4. LTP coordinates are of three types:

I. East-North-Up (ENU) coordinates shown in Figure 3.4
II. North-East-Down (NED) coordinates similar to Figure 3.4 but with Up axis pointing 'Down'wards.
III. Alpha Wander coordinates rotated from ENU coordinates through an angle α about the local vertical.

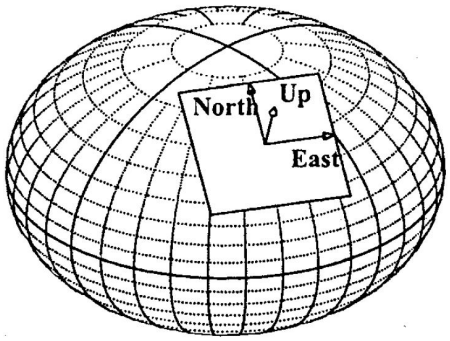

Fig 3.4: ENU (LTP) Coordinates [4]

3.3.5. Roll-Pitch-Yaw (RPY) Coordinates

RPY are vehicle fixed coordinate system. Its origin is at the Centre of Gravity of the vehicle. The direction of the movement of the vehicle is the roll axis. The orthogonal angle at the right hand side with respect to the movement of vehicle constitutes the pitch axis. The cross product of roll axis and pitch axis is the yaw axis. RPY coordinates are shown in Figure 3.5. Initially, the roll, pitch and yaw axis are aligned with NED coordinates and the attitude of the vehicle is specified in terms of angles of rotation about each of these axes. The angles of rotation about each of these axes are called Euler angles. Roll angle (R), Pitch angle (P) and Yaw angle (Y) are the rotations about the roll, pitch and yaw axis respectively. The coordinate transformation from RPY coordinates to NED coordinates can be obtained by rotating the vehicle body sequentially by Yaw angle, Pitch angle and then by Roll angle.

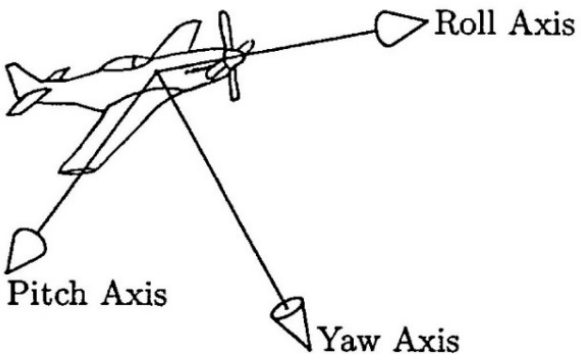

Fig 3.5: RPY Coordinates [4]

3.4. Coordinate Transformations

Coordinate Transformations from one coordinate frame to another coordinate frame is required to study INS, GNSS and their integration. The section below describes some of the basic transformations. Many other transformations between coordinate frames can be written by using the properties as given in equations (3.4)-(3.5). Readers can also use other methods of transformations such as Rotation Vectors, Direction cosine matrix and Quaternions to achieve the same, but those are beyond the scope of this thesis.

3.4.1. ENU to NED Coordinates

$$\mathbf{C}_{\text{NED}}^{\text{ENU}} = \mathbf{C}_{\text{ENU}}^{\text{NED}} = \begin{bmatrix} 0 & 1 & 0 \\ 1 & 0 & 0 \\ 0 & 0 & -1 \end{bmatrix} \tag{3.13}$$

3.4.2. ECEF to ENU Coordinates

$$X_{ENU} = \mathbf{C}_{\text{ENU}}^{\text{ECEF}} X_{ECEF} + S_{ENU} \tag{3.14}$$

Where,

$$\mathbf{C}_{\text{ENU}}^{\text{ECEF}} = \begin{bmatrix} -sin\ \theta & \cos\theta & 0 \\ -\sin\varphi\cos\theta & -\sin\varphi\ sin\ \theta & \cos\varphi \\ \cos\varphi\cos\theta & \cos\varphi\ sin\ \theta & \sin\varphi \end{bmatrix} \tag{3.15}$$

$$S_{ENU} = \begin{bmatrix} X_U \sin\theta - Y_U \cos\theta \\ X_U \sin\varphi\cos\theta - Y_U \sin\varphi\ sin\ \theta - Z_U \cos\varphi \\ -X_U \cos\varphi\cos\theta - Y_U \cos\varphi\ sin\ \theta - Z_U \sin\varphi \end{bmatrix} \tag{3.16}$$

$X_U, Y_U, Z_U =$ user' s position in ECEF coordinates

$\theta =$ local geodetic longitude

$\varphi =$ local geodetic latitude

3.4.3. RPY to NED Coordinates

To achieve RPY to NED transformation Euler angle rotations are used. Angular rotations are performed on vehicle roll, pitch and yaw axis in a specified sequence to bring the RPY coordinates to coincide with NED coordinates. The resulting transformation composed of three Euler rotation matrices.

$$\mathbf{C}_{\text{NED}}^{\text{RPY}} = \overbrace{\begin{bmatrix} C_Y & -S_Y & 0 \\ S_Y & C_Y & 0 \\ 0 & 0 & 1 \end{bmatrix}}^{\text{YAW}} \overbrace{\begin{bmatrix} C_P & 0 & S_P \\ 0 & 1 & 0 \\ -S_P & 0 & C_P \end{bmatrix}}^{\text{PITCH}} \overbrace{\begin{bmatrix} 1 & 0 & 0 \\ 0 & C_R & -S_R \\ 0 & S_R & C_R \end{bmatrix}}^{\text{ROLL}} \tag{3.17}$$

$$= \begin{bmatrix} C_Y C_P & -S_Y C_R + C_Y S_P S_R & S_Y S_R + C_Y S_P C_R \\ S_Y C_P & C_Y C_R + S_Y S_P S_R & -C_Y S_R + S_Y S_P C_R \\ -S_P & C_P S_R & C_P C_R \\ (roll\ axis) & (pitch\ axis) & (yaw\ axis) \end{bmatrix} \tag{3.18}$$

Where,

$S_R = \sin(R)$

$C_R = \cos(R)$

$S_P = \sin(P)$

$C_P = \cos(P)$

$S_Y = \sin(Y)$

$C_Y = \cos(Y)$

Euler angles are not the best way to represent vehicle attitudes specially in launching of rockets where pitch angle (*P*) is 90^0 at the time of launch. In this case, the coordinate transformations will depend only on the difference between roll angle (*R*) and yaw angle (*Y*) and a small change in vehicle yaw or pitch causes $\mp 180^0$ changes in heading angle which creates a slewing rate problem for electromechanical compasses. Representing the transformation in terms of Quaternions and Rotation Vectors are the best alternative to represent coordinate transformations.

Chapter 4

Inertial Navigation System (INS)

4.1. Fundamentals of Inertial Navigation

Inertia is the tendency of a body to preserve its current state of motion unless and until disturbed by a net external force or torque. The frame of reference, where the Newton's laws of motion are applicable, is called as the Inertial frame of reference. These frame of reference are neither accelerating nor rotating, and they are not the same as the navigation coordinates. For example, NED navigation coordinates that are used for terrestrial navigation are accelerating (to counter gravitational force) and rotating (due to earth's rotation). Such accelerations and rotations must be taken into account while designing and implementing the inertial navigation system.

Accelerometers are sensors for measuring inertial acceleration. Accelerometers do not measure gravitational acceleration, and hence it should be modeled using the software. An accelerometer fixed to a freely falling body has no detectable input. Accelerometers at rest on the surface of the earth can detect earth pushing it up but cannot detect gravity pulling it down. Gyroscopes are sensors for measuring rotation. Rate gyros measure rotation rates whereas displacement gyros measure accumulated rotation angle. Gyros forms an essential part of INS as it maintains information about the orientation of accelerometers with respect to the navigational coordinates.

Some inertial sensors when mounted rigidly to a common base forms an inertial sensor assembly (ISA) as illustrated in Figure 4.1. ISA's that are used in inertial navigation contains three accelerometers and three gyroscopes. An ISA along with its supported electronics for control and calibration is termed as inertial measurement unit (IMU). The support electronics may also include signal conditioning, thermal control, and input/output control. An IMU with Navigation computers, User interfaces, and Power supplies forms an Inertial Navigation System (INS). An INS estimates the position, velocity and attitude of its ISA.

4.2. Implementations

An INS can be implemented in two ways: Gimbaled and Strapdown implementation. Gimbaled INS use gimbal rings to isolate ISA from the rotation of vehicle as shown in Figure 4.2(a). These rings provide mechanical isolation from shocks and vibration. Further, due to isolation of sensors from high angular rates, the gimbaled INS eliminates many rate dependent sensor errors and hence its accuracy is high. Gimbaled INS can also be self-calibrated. The major disadvantages of Gimbaled INS are its cost, weight, and volume. The slip rings present can also introduce noise in the system.

Strapdown INSs are microelectromechanical systems (MEMS) and they use software to replace gimbals. The ISA is not isolated from the rotations but is mounted on the frame structure of the host vehicle as shown in Figure 4.2(b). Gyroscope maintains information about the orientation of accelerometers with respect to the navigational coordinates. External shock and vibration isolators must be provided to damp out the vibrational torques and forces transmitted to the inertial sensors. Due to high rotation rates, rate dependent sensor errors may be introduced into the system. In such cases, Gyroscopic calibration and testing are required which may increase the cost of the system. Further, Strapdown systems must operate at high rotation rates. One of the major advantages of Strapdown INS is that they are cheaper, lighter and occupies small volume as compared to Gimbaled INS and hence it is most suitable for AUV or mobile robots. This thesis mainly deals with the design and modeling of Strapdown INS only.

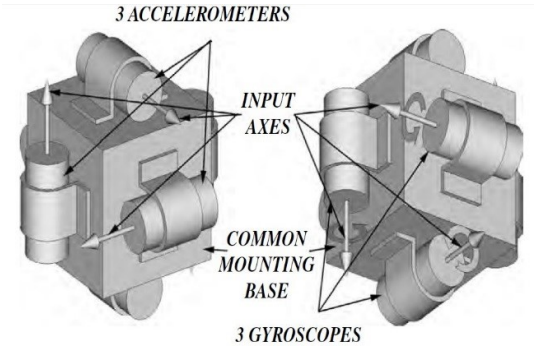

Fig 4.1: Inertial Sensor Assembly Components [4]

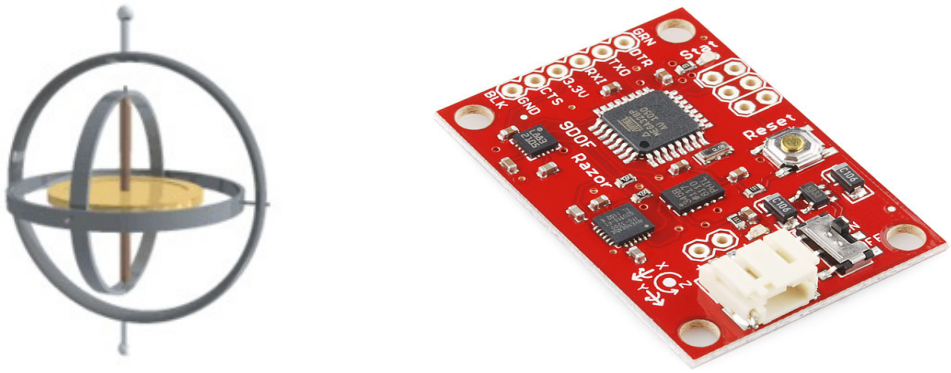

(a) Gimbaled IMU (b) Strapdown IMU

Fig 4.2: Implementation methods

4.3. Sensor Error Models

For designing a Kalman filter, the statistical properties of the errors must be known, and a mathematical model of the errors should be developed. There are three types of errors that are present in a system: Zero-mean random errors, Fixed-pattern errors, and sensor error stability.

4.3.1. *Zero-mean random errors*

- White Sensor Noise: These are generally called as electronic noise as the main sources of these types of errors are semiconductor devices and are also results of digitization. Power supplies also give rise to white noise in sensor outputs.
- Exponentially Correlated Noise: These errors look like time-varying additive noise. Variation in the temperature sensitivity of sensor bias driven by variations in ambient temperature results in exponentially correlated noise in sensor outputs.
- Random Walk Sensor Errors: These errors are characterized by an increase in the variance of errors linearly with time and decrease in power spectral density at the rate of 20dB per decade in the sensor outputs. Most navigation gyroscopes have angle random walk.
- Harmonic Noise: Temperature control schemes in Heating, Ventilating and Air Conditioning (HVAC) can introduce harmonic errors in sensor outputs due to thermal lags. Structural and suspension resonances of host vehicles can also introduce harmonic noise in sensors.

- "1/f" Noise: These errors are present in most electronic devices and is modeled as a combination of white noise and random walk. These are characterized by power spectral noise that falls off as 1/f.

4.3.2. *Fixed –Pattern errors*: Unlike the zero mean random noise, fixed pattern errors are repeatable sensor output errors. These errors include bias, scale factors, misalignment, asymmetry, nonlinearity, quantization error and a dead zone. Sensor inputs can be recovered from sensor outputs if the input-output relationship is known and invertible.

4.3.3. *Sensor Error Stability*: Fixed pattern errors doesn't remain fixed for a long period due to aging or some second order sensitivities to ambient conditions such as temperature, pressure, humidity, etc. Re-calibration and re-compensation require additional sensors that add cost. These types of errors are a serious problem in inertial navigation. These errors can be compensated to some extent by integrating INS with GNSS. This requires developing and using the models for sensor degradation patterns.

4.4. INS in One Dimension

This section is intended to provide a basic knowledge of INS. Suppose we lived in a one-dimensional world where there can be movement only along a line. There would be no rotations, and hence there is no need of gyroscope. An INS would need only one accelerometer and a navigation computer. The system can be implemented as shown in Figure 4.3. Studying the operation of INS in one dimension will make understanding of INS in three dimensions simpler.

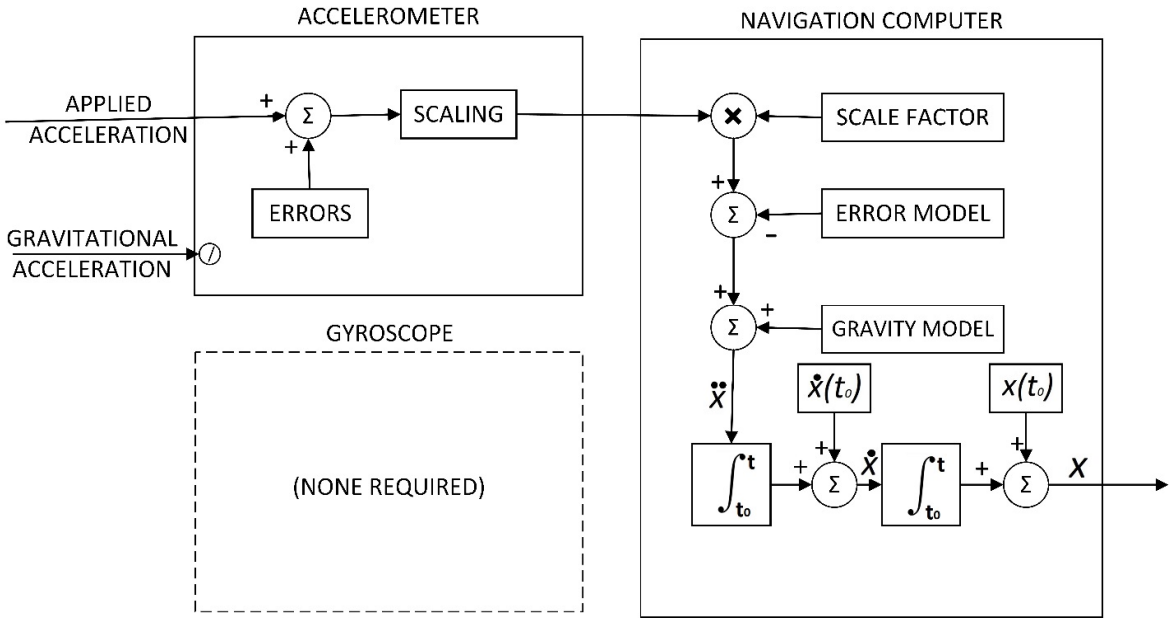

Fig 4.3: One-Dimensional INS

- Accelerometers have scale factors. Hence, the sensor output must be rescaled by multiplying by this scale factor in the navigation computer.
- Accelerometers have other errors such as constant bias, nonconstant variations in bias and scale factors, and zero mean additive noise. Constant bias can be subtracted by the same value in the navigation computer. The noise may not be predictable, but the statistical properties of the noise can be used in Kalman Filtering to eliminate zero mean additive noise and estimate drifting biases and scale factors.
- Accelerometers cannot be sensed by the accelerometer. Hence, this gravitational acceleration must be modeled and added to the sensed acceleration in the navigation computer to obtain the net acceleration $\ddot{x}$ of the INS.
- The navigation computer must integrate acceleration to obtain velocity which is a definite integral. Hence initial velocity $\dot{x}(t_0)$ of the INS must be known.
- The navigation computer must also integrate velocity to obtain position which is again a definite integral. Hence, INS must start with a known initial position $x(t_0)$ too.

4.5. INS in Nine Dimensions

In three-dimensional world, the navigation solution gives nine states as output:

- Position (three dimensional)
- Velocity (three dimensional)
- Attitude (three dimensional)

The major computational processes in Strapdown INS can be summarized by the following block diagram as shown in Figure 4.4. Note that gravitational modeling and other forms of modeling are not shown in the block diagram of Figure 4.4.

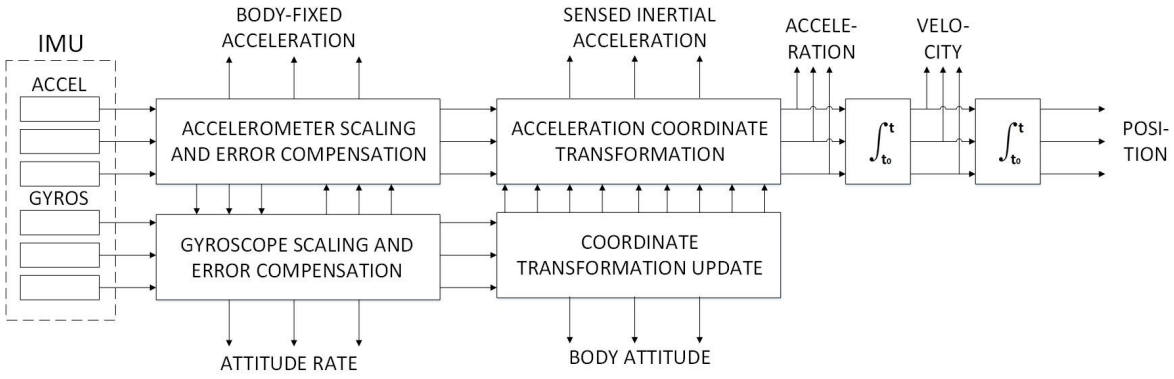

Fig 4.4: Strapdown INS

4.5.1. Navigation Coordinates

Before we proceed towards the navigation solution, it is important to define the coordinate frame where the navigation problem is to be solved. INS are mostly used for terrestrial navigation. The AUV used in our application is no exception. Therefore, the most suitable form of navigation would be to use locally level coordinates also known as LTP coordinates as defined in section 3.3.4. These could be either ENU or NED coordinate system. NED coordinates would be used for the design of navigation solution throughout the text. The advantage of using this coordinate system is that the north, east and down axes of NED coordinate system are parallel to vehicle roll, pitch and yaw axes respectively.

4.5.2. Sensor Coordinates

In Strapdown INS, sensor axes are generally aligned with the host vehicle roll, pitch and yaw axes. When the roll, pitch and yaw angles of the host vehicle are zero, RPY coordinates are

aligned with NED coordinates. For a more detailed discussion about RPY coordinates, please refer section 3.3.5.

4.5.3. Initialization

The first step of implementation of Strapdown INS is initialization of vehicle initial position, initial velocity and initial attitude in navigation coordinates. Position initialization of INS can be done through external sources such as GNSS, wireless service or manual entry. Most of the AUV vehicles starts from rest. In that case, the initial velocity of INS should be made to zero through software. If the vehicle is being carried on other vehicles, the carrier vehicle speed can be taken as reference velocity.

Determining the INS initial attitude relative to the navigation coordinates is called as INS alignment. There are four basic types of alignment techniques: Optical alignment, Gyrocompass alignment, Transfer alignment and GNSS-aided alignment. Gyrocompass alignment (Gyrocompassing) is the only form of alignment that does not rely on external sources for alignment. If integrated GNSS/INS is used, then there is no requirement of Gyrocompassing. However, most INSs are already configured for Gyrocompass alignment.

Gyrocompassing requires that the vehicle remains stationary, and any disturbances in position and attitude must be small and essentially zero mean. The alignment accuracy depends upon the time allocated for alignment and also on sensor error magnitudes. If the above conditions are met, the sensed acceleration $\mathbf{a}_{\text{output}}$ in sensor coordinates (RPY) would be in the direction of the local vertical and the sensed rotation vector $\boldsymbol{\omega}_{\text{output}}$ would be in the direction of the earth rotation axis. The unit vectors and the initial coordinate transformation can then be defined as:

$$\mathbf{1}_U = \frac{\mathbf{a}_{\text{output}}}{\left|\mathbf{a}_{\text{output}}\right|} \tag{4.1}$$

$$\mathbf{1}_N = \frac{\boldsymbol{\omega}_{\text{output}} - (\mathbf{1}_U^T \boldsymbol{\omega}_{\text{output}})\mathbf{1}_U}{\left|\boldsymbol{\omega}_{\text{output}} - (\mathbf{1}_U^T \boldsymbol{\omega}_{\text{output}})\mathbf{1}_U\right|} \tag{4.2}$$

$$\mathbf{1}_E = \mathbf{1}_N \otimes \mathbf{1}_U \tag{4.3}$$

$$\mathbf{C}_{\text{ENU}}^{\text{RPY}} = [\mathbf{1}_E \quad \mathbf{1}_N \quad \mathbf{1}_U]^T \tag{4.4}$$

Wind gusts or tides may introduce noise into the system during alignment. Gyrocompassing then requires some amount of Kalman Filtering to reduce the effects of sensor noise. The accuracy of gyrocompassing is a function of time. A highly accurate system have gyrocompassing filtering period for hours and days.

4.5.4. Sensor Calibration and Compensation

Sensor outputs in an INS are generally corrupted due to sensor biases, scale factors, and misalignments. Sensor inputs must be recovered from sensor outputs by using a compensation model. This process is known as Sensor compensation, and the process of determining the parameters of the compensation model is known as Sensor calibration. Sensor calibration is usually done at the ISA level. An affine model is used for this purpose. An affine model consists of linear part and offset part and can be written as:

$$\mathbf{z}_{\text{output}} = \mathbf{M}(\mathbf{z}_{\text{input}} + \mathbf{b}_{\text{z}}) \tag{4.5}$$

$$\mathbf{M} = \begin{bmatrix} m_{11} & m_{12} & m_{13} \\ m_{21} & m_{22} & m_{23} \\ m_{31} & m_{32} & m_{33} \end{bmatrix} \tag{4.6}$$

$\mathbf{z}_{\text{input}}$ is a vector representing inputs to three inertial sensors (either accelerometer or gyroscope). $\mathbf{z}_{\text{output}}$ is a vector representing the corresponding outputs. $\mathbf{b}_{\text{z}}$ is a vector representing sensor biases. The diagonal elements of $\mathbf{M}$ represents scale factors and off diagonal elements represents input axis misalignments. Each axis have misalignment in two orthogonal axes. The input vector can be recovered by inverting the forward model of Eq. 4.5. to obtain.

$$\mathbf{z}_{\text{input}} = \mathbf{M}^{-1}\mathbf{z}_{\text{output}} - \mathbf{b}_{\text{z}} \tag{4.7}$$

From the above equation, it can be seen that by determining the values of $\mathbf{M}$ and $\mathbf{b}_{\text{z}}$, sensor inputs can be recovered from sensor outputs. These parameters can be estimated from observations of sensor outputs when the inputs are known. For accelerometers, the inputs may include the direction and magnitude of gravity and for gyroscope inputs may include the relative direction of the rotation axis of the earth.

4.5.5. Coordinate Transformation

The inertial sensors in Strapdown INS are aligned with the vehicle roll, pitch, and yaw axes. The accelerometers measures acceleration along RPY axes. These accelerations must be projected to the NED navigation coordinates to get the navigation solution. Gyroscopes keep track of the orientation of sensors relative to NED coordinates. The transformation of acceleration from RPY coordinates to NED coordinates are achieved by using the equation 3.18. Gyroscopes measures rotation rates and, therefore, initial values of the roll, pitch and yaw angles must be known. This is achieved by comparing the Eq. 4.4 obtained from gyrocompassing with the Eq. 3.18 and solving for R, P, and Y. Another popular method to achieve this transformation is to represent attitude on the unit sphere of quaternions and using the formula derived by Bortz as described in [11].

After the accelerations are represented in NED navigation coordinates, it is easy to integrate accelerations to get velocity and integrate velocity to get position. But there are some variables that cannot be sensed and they must be calculated using the estimated values of the navigation solution. For example, gravity cannot be sensed by the accelerometer and thus it must be estimated using the estimated values of INS location and orientation and added to the sensed acceleration (NED). Similarly, there are other variables which cannot be sensed directly and must be modeled in the same way and are dealt with in detail in Section 4.8.

4.6. The Nine Core INS Error Variables

The INS measures the sum of true vehicle state and INS errors. Estimating the magnitude of errors using Kalman Filtering and subtracting it with the estimated vehicle state will give the true state of the vehicle. Navigation errors include errors in location, velocity and orientation. So the minimum dimensions of the navigation errors state will be nine. The navigation error state vector is given by

$$\boldsymbol{\zeta} = \begin{bmatrix} \varepsilon_N \\ \varepsilon_E \\ \varepsilon_D \\ \dot{\varepsilon}_N \\ \dot{\varepsilon}_E \\ \dot{\varepsilon}_D \\ \varepsilon_{\theta N} \\ \varepsilon_{\theta E} \\ \varepsilon_{\theta D} \end{bmatrix} \tag{4.8}$$

The nine navigation error state variables in NED coordinate system are

ε_N , Position error in the North direction.

ε_E , Position error in the East direction.

ε_D , Position error in the Down direction.

$\dot{\varepsilon}_N$, Velocity error in the North direction.

$\dot{\varepsilon}_E$, Velocity error in the East direction.

$\dot{\varepsilon}_D$, Velocity error in the Down direction.

$\varepsilon_{\theta N}$, Orientation error about the North axis (tilt).

$\varepsilon_{\theta E}$, Orientation error about the East axis (tilt).

$\varepsilon_{\theta D}$, Orientation error about the Down axis (heading error).

Equation 4.8 can be represented as shown in Table 4.1

Table 4.1: State variables for the Nine Core INS Errors

$\boldsymbol{\zeta}$	$\stackrel{\text{def}}{=}$	$\begin{bmatrix} \boldsymbol{\varepsilon} \\ \dot{\boldsymbol{\varepsilon}} \\ \boldsymbol{\varepsilon_\theta} \end{bmatrix}$	INS navigation error
$\boldsymbol{\varepsilon}$	$\stackrel{\text{def}}{=}$	$\begin{bmatrix} \varepsilon_N \\ \varepsilon_E \\ \varepsilon_D \end{bmatrix}$	INS location error
$\dot{\boldsymbol{\varepsilon}}$	$\stackrel{\text{def}}{=}$	$\begin{bmatrix} \dot{\varepsilon}_N \\ \dot{\varepsilon}_E \\ \dot{\varepsilon}_D \end{bmatrix}$	INS velocity error
$\boldsymbol{\varepsilon_\theta}$	$\stackrel{\text{def}}{=}$	$\begin{bmatrix} \varepsilon_{\theta N} \\ \varepsilon_{\theta E} \\ \varepsilon_{\theta D} \end{bmatrix}$	INS orientation error

4.7. Effects of Navigation Errors

Navigation errors can be divided into two categories: INS misalignment error and INS position errors.

- *Effect of INS misalignment errors*: INS misalignment represents the rotational difference between the local NED reference directions and what the navigation solution has estimated for them. INS misalignment variables are used to represent orientation errors and are different from other state variables. INS misalignment causes errors in the calculation of the direction of gravity and direction of the rotation axis of the earth, both of which are required for navigation in a rotating coordinate frame. Orientation errors involved in the miscalculation of gravity are also called as *tilt errors*. The misalignment errors get further coupled into errors in the estimation of velocity and position. This results in a complex structure. The complexity is reduced if we assume that INS sensor axes are parallel to the NED axes except for small orientation errors in the order of a milliradian or less. At those levels, error dynamics can be modeled in terms of first-order variations and second order variations can be neglected.
- *Effect of location errors*: Errors in the estimation of position results in errors in estimated latitude and longitude. A miscalculation of latitude has a direct effect on the calculation of earth rate. Errors in longitude do not have much effect on dynamic coupling of navigation errors, but they do influence pointing accuracies with respect to objects in space.

4.8. Navigation Error Dynamics

In Inertial navigation, there are some variables that cannot be sensed and they must be calculated using the estimated values of the navigation solution. For example, gravity cannot be sensed by the accelerometer and thus it must be estimated using the estimated values of INS location and orientation and added to the sensed acceleration. Similarly, there are other variables such as Coriolis acceleration, Centrifugal acceleration, leveling, etc. which cannot be sensed directly and must be modeled from the navigation solution. Correction of navigation errors is important because small errors in navigation errors get dynamically coupled to velocity errors which in turn becomes dynamically coupled with position errors.

The time-varying dynamic linear model for navigation errors will have the form,

$$\frac{d}{dt}\begin{bmatrix}\boldsymbol{\varepsilon}\\ \dot{\boldsymbol{\varepsilon}}\\ \boldsymbol{\varepsilon_\theta}\end{bmatrix}=\begin{bmatrix}\mathbf{F}_{11} & \mathbf{F}_{12} & \mathbf{F}_{13}\\ \mathbf{F}_{21} & \mathbf{F}_{22} & \mathbf{F}_{23}\\ \mathbf{F}_{31} & \mathbf{F}_{32} & \mathbf{F}_{33}\end{bmatrix}\begin{bmatrix}\boldsymbol{\varepsilon}\\ \dot{\boldsymbol{\varepsilon}}\\ \boldsymbol{\varepsilon_\theta}\end{bmatrix} \tag{4.9}$$

where

$\mathbf{F}_{11}$ represents the dynamic coupling of location errors into location errors

$\mathbf{F}_{12}$ represents the dynamic coupling of velocity errors into location errors

$\mathbf{F}_{13}$ represents the dynamic coupling of orientation errors into location errors

$\mathbf{F}_{21}$ represents the dynamic coupling of location errors into velocity errors

$\mathbf{F}_{22}$ represents the dynamic coupling of velocity errors into velocity errors

$\mathbf{F}_{23}$ represents the dynamic coupling of orientation errors into velocity errors

$\mathbf{F}_{31}$ represents the dynamic coupling of location errors into orientation errors

$\mathbf{F}_{32}$ represents the dynamic coupling of velocity errors into orientation errors

$\mathbf{F}_{33}$ represents the dynamic coupling of orientation errors into orientation errors

There are seven factors that need to be considered for modeling. These include:

a) Integration of velocities
b) Estimation of gravity
c) Misalignment (Attitude errors)
d) Coriolis Acceleration
e) Location errors
f) Earth rate leveling
g) Velocity leveling

The complete dynamic coefficient matrix would be the sum of contributions from all seven. Mathematical models for each of the seven are described below.

4.8.1. *Error Dynamics due to Integration of Velocities*: INS location cannot be measured directly, and it must be inferred from the integration of velocities. Any errors in estimated velocity will also be integrated and would add to location errors. Hence, velocity errors are dynamically coupled into location errors. This can be modeled as:

$$\frac{d}{dt}\varepsilon=\dot{\varepsilon} \tag{4.10}$$

$$\mathbf{F}_{11} = 0\ (3\ \times 3\ zero\ matrix) \tag{4.11}$$

$$\mathbf{F}_{12} = \mathbf{I}\ (3 \times 3\ Identity\ matrix \tag{4.12}$$

$$\mathbf{F}_{13} = 0\ (3\ \times 3\ zero\ matrix) \tag{4.13}$$

4.8.2. *Error Dynamics due to Gravity Calculations*: Gravity cannot be sensed by the accelerometer and hence it must be calculated using the navigation solution. The errors due to gravity miscalculations when the INS is at rest can be modeled as:

$$\frac{d}{dt}\begin{bmatrix}\dot{\varepsilon}_N\\ \dot{\varepsilon}_E\\ \dot{\varepsilon}_D\end{bmatrix} = \begin{bmatrix}0 & g & 0\\ -g & 0 & 0\\ 0 & 0 & 0\end{bmatrix}\begin{bmatrix}\varepsilon_{\theta N}\\ \varepsilon_{\theta E}\\ \varepsilon_{\theta D}\end{bmatrix} \tag{4.14}$$

$$\mathbf{F}_{23[1]} = \begin{bmatrix}0 & g & 0\\ -g & 0 & 0\\ 0 & 0 & 0\end{bmatrix} \tag{4.15}$$

4.8.3. *Error Dynamics due to Misalignment*: As explained earlier, INS misalignment causes errors in the calculation of the direction of gravity and direction of the rotation axis of the earth. These effects are modeled by using the first order small angle rotation error matrix

$$[\boldsymbol{\varepsilon}_{\boldsymbol{\theta}}] = \begin{bmatrix}0 & -\varepsilon_{\theta D} & \varepsilon_{\theta E}\\ \varepsilon_{\theta D} & 0 & -\varepsilon_{\theta N}\\ -\varepsilon_{\theta E} & \varepsilon_{\theta N} & 0\end{bmatrix} \tag{4.16}$$

When sensed accelerations are represented in terms of navigation accelerations, errors in estimated attitude cause errors in estimated acceleration. Sensed acceleration can be written as:

$$a_{SENSED} = \begin{bmatrix}a_N\\ a_E\\ a_D\end{bmatrix} \tag{4.17}$$

The errors can then be modeled as

$$\frac{d}{dt}\begin{bmatrix}\dot{\varepsilon}_N\\ \dot{\varepsilon}_E\\ \dot{\varepsilon}_D\end{bmatrix} \approx \begin{bmatrix}0 & -\varepsilon_{\theta D} & \varepsilon_{\theta E}\\ \varepsilon_{\theta D} & 0 & -\varepsilon_{\theta N}\\ -\varepsilon_{\theta E} & \varepsilon_{\theta N} & 0\end{bmatrix}\begin{bmatrix}a_N\\ a_E\\ a_D + g\end{bmatrix} \tag{4.18}$$

$$\approx \begin{bmatrix}0 & a_D + g & -a_N\\ -a_D - g & 0 & a_E\\ a_N & -a_E & 0\end{bmatrix}\begin{bmatrix}\varepsilon_{\theta N}\\ \varepsilon_{\theta E}\\ \varepsilon_{\theta D}\end{bmatrix} \tag{4.19}$$

$$\mathbf{F}_{23[2]} = \begin{bmatrix}0 & a_D + g & -a_N\\ -a_D - g & 0 & a_E\\ a_N & -a_E & 0\end{bmatrix} \tag{4.20}$$

$$\mathbf{F}_{23} = \mathbf{F}_{23[1]} + \mathbf{F}_{23[2]} \tag{4.21}$$

$$\mathbf{F}_{23} = \begin{bmatrix} 0 & a_D + 2g & -a_N \\ -a_D - 2g & 0 & a_E \\ a_N & -a_E & 0 \end{bmatrix} \tag{4.22}$$

When the INS is at rest, the sensed acceleration is given by,

$$a_{SENSED} = \begin{bmatrix} 0 \\ 0 \\ -g \end{bmatrix} \tag{4.23}$$

and Equations 4.22 and 4.15 becomes identical.

4.8.4. *Error Dynamics due to Coriolis Acceleration*: Coriolis Accelerations cannot be sensed either and hence it must be estimated from the navigation solution. The apparent acceleration due to Coriolis effect in rotating coordinates is given by,

$$a_{Coriolis} = -2\Omega \otimes V \tag{4.24}$$

where $a_{Coriolis}$ is the Coriolis acceleration, $\otimes$ is the vector cross product, V is the velocity in rotating coordinates and Ω is the coordinate rotation rate vector

$$\Omega = \Omega_{\odot} \begin{bmatrix} \cos(\lambda) \\ 0 \\ -\sin(\lambda) \end{bmatrix} \tag{4.25}$$

$$\Omega_{\odot} \approx 7.292115 \times 10^{-5}\, rad/s \tag{4.26}$$

λ =latitude of INS location

$$\frac{d}{dt}\begin{bmatrix} \dot{\varepsilon}_N \\ \dot{\varepsilon}_E \\ \dot{\varepsilon}_D \end{bmatrix} = \begin{bmatrix} 0 & -2\Omega_{\odot}\sin(\lambda) & 0 \\ 2\Omega_{\odot}\sin(\lambda) & 0 & 2\Omega_{\odot}\cos(\lambda) \\ 0 & -2\Omega_{\odot}\cos(\lambda) & 0 \end{bmatrix}\begin{bmatrix} \dot{\varepsilon}_N \\ \dot{\varepsilon}_E \\ \dot{\varepsilon}_D \end{bmatrix} \tag{4.27}$$

$$\mathbf{F}_{22} = \begin{bmatrix} 0 & -2\Omega_{\odot}\sin(\lambda) & 0 \\ 2\Omega_{\odot}\sin(\lambda) & 0 & 2\Omega_{\odot}\cos(\lambda) \\ 0 & -2\Omega_{\odot}\cos(\lambda) & 0 \end{bmatrix} \tag{4.28}$$

4.8.5. *Error Dynamics due to Location Errors*: Miscalculation of position of the INS can dynamically couple navigation errors into velocity errors and is represented by,

$$\frac{d}{dt}\begin{bmatrix} \dot{\varepsilon}_N \\ \dot{\varepsilon}_E \\ \dot{\varepsilon}_D \end{bmatrix} \approx \begin{bmatrix} -\tau_S^{-2} & 0 & 0 \\ 0 & -\tau_S^{-2} & 0 \\ 0 & 0 & \tau_D^{-2} \end{bmatrix}\begin{bmatrix} \varepsilon_N \\ \varepsilon_E \\ \varepsilon_D \end{bmatrix} \tag{4.29}$$

$$\tau_S \approx 806.4\, s$$

$$\tau_D \approx 520\, s$$

$$\mathbf{F}_{21} = \begin{bmatrix} -\tau_S^{-2} & 0 & 0 \\ 0 & -\tau_S^{-2} & 0 \\ 0 & 0 & \tau_D^{-2} \end{bmatrix} \tag{4.30}$$

4.8.6. *Error Dynamics due to Earth rate Leveling*: Leveling is the process of maintaining a locally level reference frame for terrestrial navigation. An INS senses rotation rates even when it is kept at rest on the surface of the earth due to earth's rotation. Based on the navigation solution for orientation and latitude, an INS must estimate the contribution due to earth rotation rate and subtract it to maintain it's locally level orientation.

$$\frac{d}{dt}\begin{bmatrix} \varepsilon_{\theta N} \\ \varepsilon_{\theta E} \\ \varepsilon_{\theta D} \end{bmatrix} \approx \begin{bmatrix} 0 & -\varepsilon_{\theta D} & \varepsilon_{\theta E} \\ \varepsilon_{\theta D} & 0 & -\varepsilon_{\theta N} \\ -\varepsilon_{\theta E} & \varepsilon_{\theta N} & 0 \end{bmatrix} \begin{bmatrix} \Omega_{\odot}\cos(\lambda) \\ 0 \\ -\Omega_{\odot}\sin(\lambda) \end{bmatrix} \tag{4.31}$$

$$\approx \begin{bmatrix} 0 & -\Omega_{\odot}\sin(\lambda) & 0 \\ \Omega_{\odot}\sin(\lambda) & 0 & \Omega_{\odot}\cos(\lambda) \\ 0 & -\Omega_{\odot}\cos(\lambda) & 0 \end{bmatrix} \begin{bmatrix} \varepsilon_{\theta N} \\ \varepsilon_{\theta E} \\ \varepsilon_{\theta D} \end{bmatrix} \tag{4.32}$$

$$\mathbf{F}_{33} = \begin{bmatrix} 0 & -\Omega_{\odot}\sin(\lambda) & 0 \\ \Omega_{\odot}\sin(\lambda) & 0 & \Omega_{\odot}\cos(\lambda) \\ 0 & -\Omega_{\odot}\cos(\lambda) & 0 \end{bmatrix} \tag{4.33}$$

4.8.7. *Error Dynamics due to Velocity Leveling*: Leveling is also required while the INS moves over the curved surface of the earth. A miscalculation of this correction will dynamically couple velocity errors into orientation errors.

$$\frac{d}{dt}\begin{bmatrix} \varepsilon_{\theta N} \\ \varepsilon_{\theta E} \\ \varepsilon_{\theta D} \end{bmatrix} = \begin{bmatrix} 0 & R_{\odot}^{-1} & 0 \\ -R_{\odot}^{-1} & 0 & 0 \\ 0 & 0 & 0 \end{bmatrix} \begin{bmatrix} \dot{\varepsilon}_N \\ \dot{\varepsilon}_E \\ \dot{\varepsilon}_D \end{bmatrix} \tag{4.34}$$

$$R_{\odot} = Mean\ radius\ of\ Earth = 6372795.5\ m$$

$$\mathbf{F}_{32} = \begin{bmatrix} 0 & R_{\odot}^{-1} & 0 \\ -R_{\odot}^{-1} & 0 & 0 \\ 0 & 0 & 0 \end{bmatrix} \tag{4.35}$$

4.8.8. Contributions from all the Factors

Considering all the factors from Equations 4.11, 4.12, 4.13, 4.22, 4.28, 4.30, 4.33, 4.35 and putting it in the Equation 4.9, we get a 9 x 9 Dynamic Coefficient Matrix for INS navigation errors which can be written as,

$$F_{NN} = \begin{bmatrix} 0 & 0 & 0 & 1 & 0 & 0 & 0 & 0 & 0 \\ 0 & 0 & 0 & 0 & 1 & 0 & 0 & 0 & 0 \\ 0 & 0 & 0 & 0 & 0 & 1 & 0 & 0 & 0 \\ -\tau_S^{-2} & 0 & 0 & 0 & -2\Omega_\odot s_\lambda & 0 & 0 & a_D + 2g & -a_N \\ 0 & -\tau_S^{-2} & 0 & 2\Omega_\odot s_\lambda & 0 & 2\Omega_\odot c_\lambda & -a_D - 2g & 0 & a_E \\ 0 & 0 & \tau_D^{-2} & 0 & -2\Omega_\odot c_\lambda & 0 & a_N & -a_E & 0 \\ 0 & 0 & 0 & 0 & R_\odot^{-1} & 0 & 0 & -\Omega_\odot s_\lambda & 0 \\ 0 & 0 & 0 & -R_\odot^{-1} & 0 & 0 & \Omega_\odot s_\lambda & 0 & \Omega_\odot c_\lambda \\ 0 & 0 & 0 & 0 & 0 & 0 & 0 & -\Omega_\odot c_\lambda & 0 \end{bmatrix} \quad (4.36)$$

$\tau_S = 806.4\ s\ (Schuler\ time - constant)$

$\tau_D = 520\ s\ (Vertical\ channel\ time - constant)$

$g = 9.8\ m/s^2\ (\ Acceleration\ due\ to\ gravity)$

$R_\odot = 6372795.5\ m\ (Radius\ of\ the\ Earth)$

$\Omega_\odot = 7.292115\ \times\ 10^{-5} rad/s\ (\ Rotation\ rate\ of\ earth)$

$\lambda = INS\ latitude$

$s_\lambda = \sin(\lambda)$

$c_\lambda = \cos(\lambda)$

$a_N = north\ component\ of\ INS\ acceleration\ [m/s^2]$

$a_E = east\ component\ of\ \ INS\ acceleration\ [m/s^2]$

$a_D = down\ component\ of\ INS\ acceleration\ [m/s^2]$

4.9. Analysis of Dynamic Coefficient Matrix

4.9.1. Schuler Oscillations

Tilts or orientation errors are results of initial INS alignment errors. It arises due to errors in estimated direction of gravity in the local coordinate frame. The translation of tilts into navigation errors is through a process called Schuler oscillation. This process is better explained using an analogy between a simple gravity pendulum and INS Earth pendulum model as illustrated in Figure 4.5. The net force acting on a pendulum is the resultant of Tension T and the mass weight (mg) as shown in figure 4.5(a). This model can be extended to INS Earth pendulum model whose pivot is the center of the earth and the mass being the INS itself as shown in figure 4.5(b). The net force acting on this analogous pendulum is the resultant of modeled acceleration of gravity (through software) and the sensed gravitational

acceleration. However, it should be remembered that gravity pendulum is a physical device whereas earth pendulum is a theoretical model developed to explain how INS orientation errors translate into navigation errors. In gravity pendulum, the mass of the pendulum oscillates whereas in earth pendulum model, it is the INS errors such as estimated position, velocity and acceleration errors that oscillate.

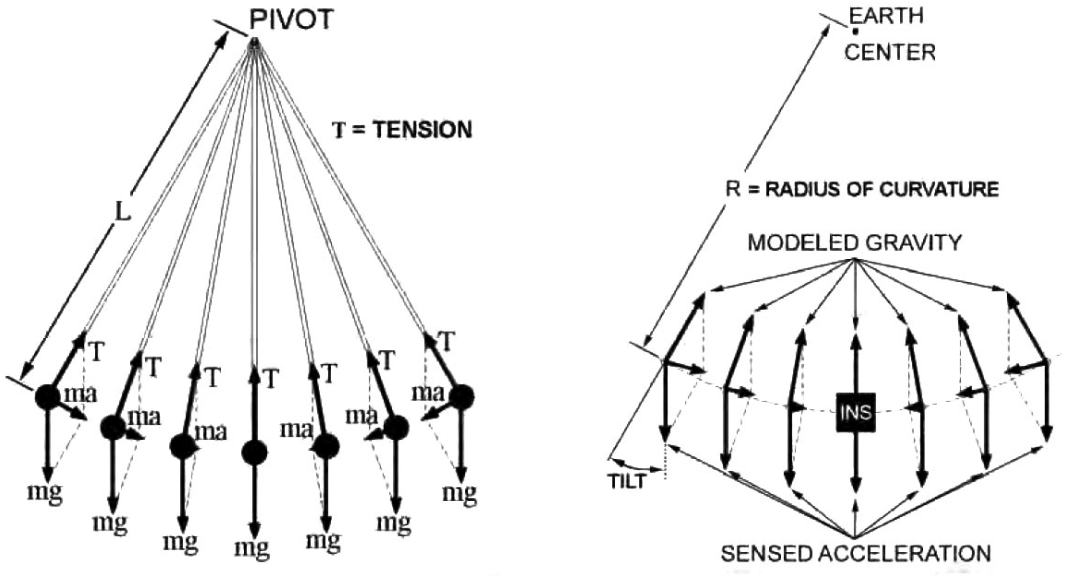

(a) A Gravity, Pendulum model (b) INS Earth Pendulum model

Fig 4.5: Pendulum model for Schuler Oscillation [4]

In the case of the gravity pendulum, the period of oscillation is,

$$T = \frac{2\pi}{\omega} = \frac{2\pi\sqrt{L}}{\sqrt{g}} \tag{4.37}$$

And for the Schuler pendulum at the surface of the earth,

$$T_{Schuler} = \frac{2\pi\sqrt{R}}{\sqrt{g}} \approx 84.4\ min \tag{4.38}$$

This 84.4 min period is called as the Schuler period. Figure 4.6 is a plot generated using the Dynamic Coefficient matrix of Eq. 4.36. This plot shows how a small initial north velocity error give rise to Schuler oscillation. Apart from oscillating, the direction of oscillation also rotates making the oscillation look like those of Foucault pendulum. This is due to Coriolis accelerations. The observation of Schuler oscillations is the classic pattern of behavior for INS errors. During INS development and testing, it is standard practice to induce horizontal

velocity errors in INS to verify its software implementation by observing the resulting Schuler oscillation pattern.

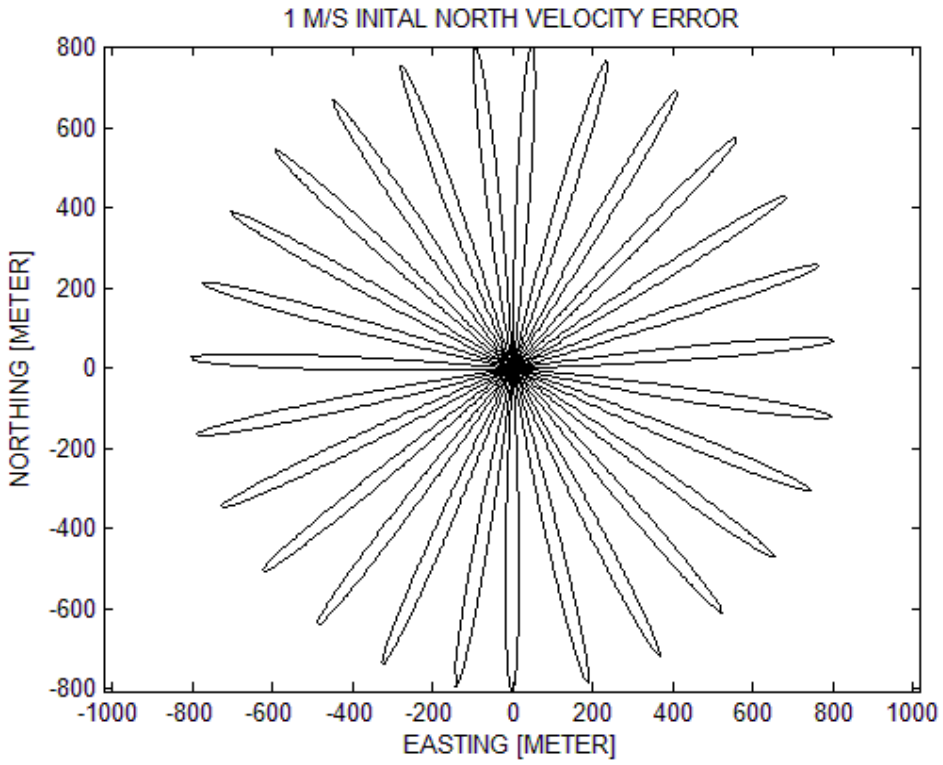

Fig 4.6: Schuler Oscillation with North Velocity Error

4.9.2. Sensitivity to Accelerometer Errors

Inertial navigation is relatively insensitive to additive zero-mean white sensor noise as the sensor outputs are integrated throughout the entire operation of INS. However, if the errors are not zero-mean over long periods of time, small errors can result in large output errors. For example, a very small constant accelerometer output error,

$$\varepsilon_a = 10^{-5} g = 9.8 \times 10^{-5}\, m/s^2 \tag{4.39}$$

doubly integrated for 2 hours (7200 s) produces a position error of

$$\varepsilon_p = 0.5 \times \varepsilon_a \times (7200)^2 = 2.5\, km \tag{4.40}$$

which is larger than RMS position errors from GNSS navigation by more than two orders. We will simulate the above conditions ($10^{-5} g$ accelerometer bias error) using MATLAB to see how the simple integration model computed above compares with a more complete model of INS errors of Eq. 4.36. Figure 4.7 is a set of plots generated by simulating a north accelerometer bias error of $10^{-5} g$ for 1 hour. It shows about one cycle of Schuler oscillation

in north position error with a peak-to-peak variation of the order of 70 m, plus some Coriolis coupling into the east and vertical directions. From the attitude error, we can also infer that the errors in the vertical direction are unstable and hence some type of aiding is required in the vertical direction. The peak error is far less than predicted by the simple model computed above but still bigger than RMS GNSS navigation errors.

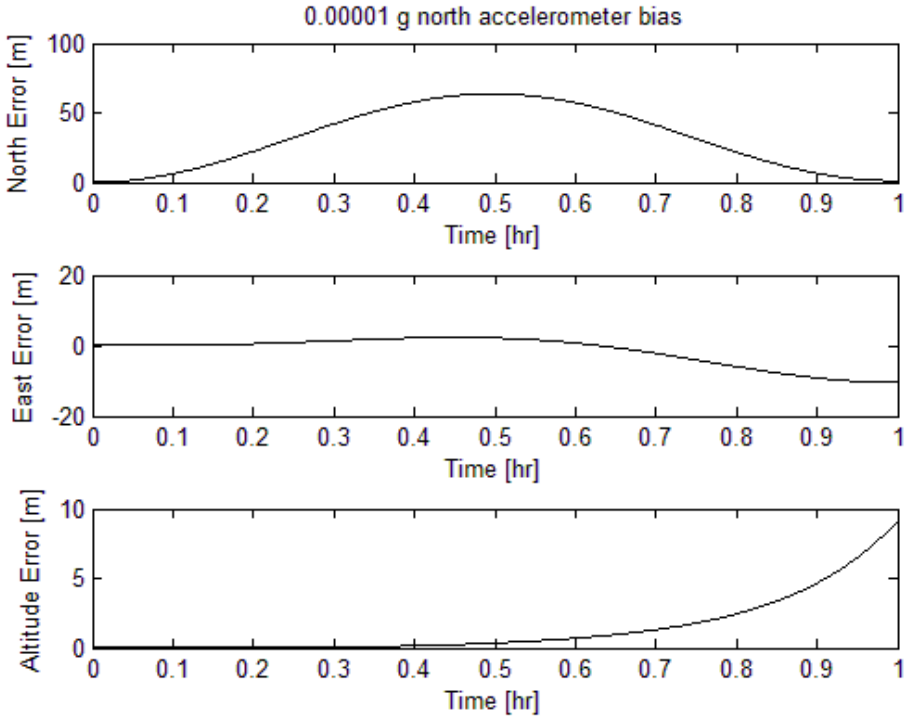

Fig 4.7: Simulated INS errors from north accelerometer bias

4.9.3. Vertical Error Instability

Newton's universal law of gravitation is an inverse-square law. For a vehicle at a height h above the surface of the earth with radius $R_\odot$ the calculated downward acceleration is

$$g = \frac{GM_\odot}{(R_\odot + h)^2} \tag{4.41}$$

where $M_\odot$ is the mass of the earth and G is the universal gravitational constant. If the error in estimated height is ε_D(measured downward), then the error in calculated gravitational acceleration will be $\ddot{\varepsilon}_D$, where

$$g + \ddot{\varepsilon}_D = \frac{GM_\odot}{(R_\odot + h - \varepsilon_D)^2} \tag{4.42}$$

Differentiating it with respect to h, we will get

$$\ddot{\varepsilon}_D \approx [-\frac{\partial g}{\partial h}\Big|_{\varepsilon_D=0}]\,\varepsilon_D \tag{4.43}$$

$$\ddot{\varepsilon}_D \approx 2\frac{g}{R_\odot}\varepsilon_D \; for \; |h| \ll R_\odot \tag{4.44}$$

$$\ddot{\varepsilon}_D \approx \tau_D^{-2}\varepsilon_D \tag{4.45}$$

Where,

$$\tau_D = \sqrt{\frac{R_\odot}{2 \times g}} = 570\ s \tag{4.46}$$

The solution to which is exponentially unstable.

$$\varepsilon_D(t) = \varepsilon_D(t_0)\exp(\frac{t-t_0}{\tau_D}) \tag{4.47}$$

Vehicles that does not need to navigate in the vertical direction such as ships at sea, instability of INS errors in the vertical direction is not a problem. But for vehicles such as AUV, aircraft, submarines, etc. some form of auxiliary sensor aiding is required to control vertical INS errors. Altimeter, Pressure sensor or GNSS can be used in addition to INS for this purpose.

Stabilization of Vertical altitude of an INS can be done with the help of a barometer. For this example, the barometer is assumed to have an RMS altitude error of 100 m with a correlation time-constant of 8 hours, plus RMS white noise of 10 m. The INS is assumed to be driven by RMS position process noise of 1 cm, velocity process noise of 1 μg per sample interval of 1 s and attitude process noise of 0.01 deg/h RMS [3].

For designing a Kalman filter, statistical and dynamical information of the errors must be available. The errors in barometer are exponentially correlated. The exponentially correlated processes can be modeled as,

$$\dot{\varepsilon}_{bar} = -\frac{\varepsilon_{bar}}{\tau_{bar}} + w_{bar}(t) \tag{4.48}$$

Where τ_{bar} is the exponentially correlation time of the barometer errors, $w_{bar}(t)$ is a zero mean white noise process with variance,

$$q_{bar} = \frac{2\sigma_{bar}^2}{\tau_{bar}} \tag{4.49}$$

and σ_{bar}^2 is the mean squared barometric error. The measurement noise is given by,

$$r_{bar} = \sigma_{bar}^2 \tag{4.50}$$

Dynamic Coefficient Matrix for the augmented system will have the form,

$$F_{Aug} = \begin{bmatrix} F_{NN} & 0 \\ 0 & -1/\tau_{bar} \end{bmatrix} \tag{4.51}$$

The barometer output error is the sum of altitude measured through INS errors and the slowly varying barometer noise. The measurement sensitivity matrix for the barometer output has the form,

$$\mathbf{H}_{bar} = [0 \quad 0 \quad 1 \quad 0 \quad 0 \quad 0 \quad 0 \quad 0 \quad 0 \quad 1] \tag{4.52}$$

Kalman filter was designed using Equations 4.49 through 4.52 and was implemented in MATLAB. The variation of RMS altitude uncertainty with time is shown in Figure 4.8. For the aided case, the RMS altitude uncertainty is quite stable, and it settles to about less than 1m even after one hour of operation. For the unaided case, the RMS altitude uncertainty rises to around 30 km in one hour. Hence, the vertical instability can be stabilized by using external aiding coupled with INS through Kalman Filtering.

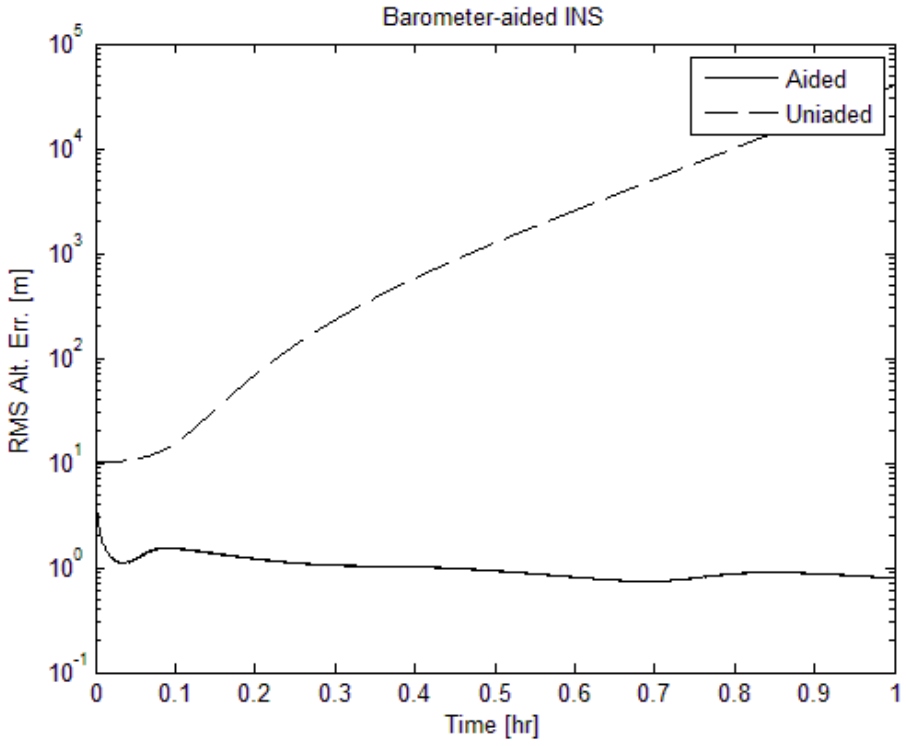

Fig 4.8: Barometer aided INS altitude uncertainties

4.10. Inertia Sensor Noise

After the sensor compensation has been done, the errors that still remain in the process are the zero mean white noise from the accelerometers and gyroscopes as explained in Section 4.4. The navigation error dynamic model has the form,

$$\frac{d}{dt}\boldsymbol{\zeta} = F_{NN}\boldsymbol{\zeta} + w_{sensor}(t) \tag{4.53}$$

The white noise from the accelerometers is integrated into velocity errors, and the white noise from gyroscopes is integrated into orientation errors. The process noise covariance will then have the covariance structure,

$$\mathbf{Q}_{sen\_noise} \overset{\text{def}}{=} E\langle w_{sensor}(t) w_{sensor}^{T}(t)\rangle \tag{4.54}$$

$$= \begin{bmatrix} 0 & 0 & 0 \\ 0 & \mathbf{Q}_{acc} & 0 \\ 0 & 0 & \mathbf{Q}_{gyro} \end{bmatrix} \tag{4.55}$$

where $\mathbf{Q}_{acc}$ is the accelerometer noise covariance and $\mathbf{Q}_{gyro}$ is the gyro noise covariance. Assuming that there is no noise correlation between sensors and accelerometer noise variance is the same for all accelerometers and gyro noise covariance is also the same for all gyros, these submatrices can be written as,

$$\mathbf{Q}_{acc} = q_{acc}\mathbf{I} \tag{4.56}$$

$$\mathbf{Q}_{gyro} = q_{gyro}\mathbf{I} \tag{4.57}$$

4.11. Sensor Error Models

Sensor error modeling is used in a number of ways in INS. Manufacturers often test their sensors and distribute their models of error characteristics to be used by INS designers. These models are used to predict and control the accuracy levels, dynamic ranges and other error mechanisms of accelerometers and gyroscopes. These same models can be used for implementation of integrated GNSS/INS with Kalman Filtering for recalibration and compensation of drifting sensor errors during navigation.

First-order sensor errors of INS sensors include biases (one per sensor), scale factor variations (one per sensor) and input axis misalignments (two per sensor).

The first-order model for inertial sensor errors has the form

$$y_{output} = Ly_{input} + b_y \tag{4.58}$$

$$L = \begin{bmatrix} S_{XX} & M_{XY} & M_{XZ} \\ M_{YX} & S_{YY} & M_{YZ} \\ M_{ZX} & M_{ZY} & S_{ZZ} \end{bmatrix} \tag{4.59}$$

In the above equation, y represents either accelerations (for accelerometers) or rotation rates (for gyroscopes), y_{input} is the vector of input values, y_{output} is the vector of output values, and b_y is the vector of sensor biases. The matrix L is called the scale factor and misalignment matrix. The diagonal terms S_{ii} of L represent sensor scale factors and the off-diagonal terms M_{ij} represent sensor input axis misalignments. The elements of L and b_y are the model parameters.

Each sensor has two axes of freedom for input axis misalignment, which adds up to a total of twelve degrees of freedom for six sensor assembly (three accelerometers and three gyroscopes). However, three out of twelve degrees of freedom are unobservable sensor misalignment which are due to rigid body rotations of the ISA and are part of INS error model. That leaves only nine degrees of freedom in input axis misalignment.

The sensor error state vector is given by

$$\varepsilon_{INSSENS} = \begin{bmatrix} x_a \\ x_g \end{bmatrix} \tag{4.60}$$

$$x_a = \begin{bmatrix} \varepsilon_{abX} \\ \varepsilon_{abY} \\ \varepsilon_{abZ} \\ \varepsilon_{asX} \\ \varepsilon_{asY} \\ \varepsilon_{asZ} \\ \varepsilon_{aYZs} \\ \varepsilon_{aZXs} \\ \varepsilon_{aXYs} \end{bmatrix} \tag{4.61}$$

$$x_g = \begin{bmatrix} \varepsilon_{gbX} \\ \varepsilon_{gbY} \\ \varepsilon_{gbZ} \\ \varepsilon_{gsX} \\ \varepsilon_{gsY} \\ \varepsilon_{gsZ} \\ \varepsilon_{gYZs} \\ \varepsilon_{gZXs} \\ \varepsilon_{gXYs} \\ \varepsilon_{gYZa} \\ \varepsilon_{gZXa} \\ \varepsilon_{gXYa} \end{bmatrix} \tag{4.62}$$

$\varepsilon_{abX}, \varepsilon_{abY}, \varepsilon_{abZ}$ are the accelerometer bias errors.

$\varepsilon_{asX}, \varepsilon_{asY}, \varepsilon_{asZ}$ are the accelerometer scale factor errors.

$\varepsilon_{aYZs}, \varepsilon_{aZXs}, \varepsilon_{aXYs}$ are the accelerometer input axis misalignment errors.

$\varepsilon_{gbX}, \varepsilon_{gbY}, \varepsilon_{gbZ}$ are the gyroscope bias errors.

$\varepsilon_{gsX}, \varepsilon_{gsY}, \varepsilon_{gsZ}$ are the gyroscope scale factor errors.

$\varepsilon_{gYZs}, \varepsilon_{gZXs}, \varepsilon_{gXYs}, \varepsilon_{gYZa}, \varepsilon_{gZXa}, \varepsilon_{gXYa}$ are the gyroscope input axis misalignment errors.

4.11.1. Sensor Compensation Error Models

Inertial navigation requires extreme sensor accuracy. This cannot be achieved through manufacturing precision alone. The errors can be adequately compensated using sensor calibration models during navigation. However, it is very likely that the compensation parameters change a little during operation. Additional sensors such as GNSS can be used for INS sensor recalibration during navigation. The models for sensor recalibration are developed in the following section.

Slowly varying sensor compensation error models for an ISA are usually exponentially correlated process models or random walk models. The dynamic model used here is of independent, exponentially correlated process that has the form

$$\frac{d}{dt}\varepsilon = \frac{-1}{\tau}\varepsilon + w(t) \tag{4.63}$$

Where τ is the specified correlation time constant and is $w(t) \in \mathcal{N}(0,2\sigma\text{^}2/\tau)$. $\sigma^2 = E\langle\varepsilon^2\rangle$ is the mean squared sensor error.

For the 21 sensor error state variables defined in Equation 4.60, the above equation will have the form

$$\frac{d}{dt}\varepsilon_{INSSENS} = F_{ss}\varepsilon_{INSSENS} + w_{drift}(t) \tag{4.64}$$

$$F_{ss} = \begin{bmatrix} -\tau_{abX}^{-1} & 0 & 0 & 0 & 0 & 0 & \cdots & 0 & 0 & 0 \\ 0 & -\tau_{abY}^{-1} & 0 & 0 & 0 & 0 & \cdots & 0 & 0 & 0 \\ 0 & 0 & -\tau_{abZ}^{-1} & 0 & 0 & 0 & \cdots & 0 & 0 & 0 \\ 0 & 0 & 0 & -\tau_{asX}^{-1} & 0 & 0 & \cdots & 0 & 0 & 0 \\ 0 & 0 & 0 & 0 & -\tau_{asY}^{-1} & 0 & \cdots & 0 & 0 & 0 \\ 0 & 0 & 0 & 0 & 0 & -\tau_{asZ}^{-1} & \cdots & 0 & 0 & 0 \\ \vdots & \vdots & \vdots & \vdots & \vdots & \vdots & \ddots & \vdots & \vdots & \vdots \\ 0 & 0 & 0 & 0 & 0 & 0 & \cdots & -\tau_{gYZa}^{-1} & 0 & 0 \\ 0 & 0 & 0 & 0 & 0 & 0 & \cdots & 0 & -\tau_{gZXa}^{-1} & 0 \\ 0 & 0 & 0 & 0 & 0 & 0 & \cdots & 0 & 0 & -\tau_{gXYa}^{-1} \end{bmatrix} \tag{4.65}$$

And the corresponding 21 x 21 covariance matrix

$$\mathbf{Q}_{drift} \stackrel{\text{def}}{=} E\langle w_{drift}(t) w_{drift}^{T}(t)\rangle = \begin{bmatrix} 2\sigma_{abX}^2/\tau_{abX} & 0 & 0 & \cdots & 0 \\ 0 & 2\sigma_{abY}^2/\tau_{abY} & 0 & \cdots & 0 \\ 0 & 0 & 2\sigma_{abZ}^2/\tau_{abZ} & \cdots & 0 \\ \vdots & \vdots & \vdots & \ddots & \vdots \\ 0 & 0 & 0 & \cdots & 2\sigma_{gXYa}^2/\tau_{gXYa} \end{bmatrix} \tag{4.66}$$

The models derived above assumed that the sensor errors are independent of each other. However, a model derived using experimental data may have correlations among the sensor errors. These data can be used to enhance the performance of GNSS/INS sensor fusion.

4.11.2. Dynamic Coupling into Navigation Errors

Navigation errors do not dynamically couple into sensor errors, but the sensor errors do couple directly into the time derivatives of navigation errors. Due to compensation errors, the errors in navigation dynamics can be modeled by a first-order model as,

$$\frac{d}{dt}\begin{bmatrix} \dot{\varepsilon}_N \\ \dot{\varepsilon}_E \\ \dot{\varepsilon}_D \end{bmatrix} = C_{NED}^{XYZ}\left\{\begin{bmatrix} \varepsilon_{abX} \\ \varepsilon_{abY} \\ \varepsilon_{abZ} \end{bmatrix} + [\varepsilon_{aL}]a_{sensed}\right\} \tag{4.67}$$

$$\frac{d}{dt}\begin{bmatrix}\varepsilon_{\theta N}\\ \varepsilon_{\theta E}\\ \varepsilon_{\theta D}\end{bmatrix} = C_{NED}^{XYZ}\left\{\begin{bmatrix}\varepsilon_{gbX}\\ \varepsilon_{gbY}\\ \varepsilon_{gbZ}\end{bmatrix} + [\varepsilon_{gL}]\omega_{sensed}\right\} \tag{4.68}$$

$$[\varepsilon_{aL}] = \begin{bmatrix}\varepsilon_{asX} & \varepsilon_{aXYs} & \varepsilon_{aZXs}\\ \varepsilon_{aXYs} & \varepsilon_{asY} & \varepsilon_{aYZs}\\ \varepsilon_{aZXs} & \varepsilon_{aYZs} & \varepsilon_{asZ}\end{bmatrix} \tag{4.69}$$

$$[\varepsilon_{gL}] = \begin{bmatrix}\varepsilon_{gsX} & \varepsilon_{gXYs} - \varepsilon_{gXYa} & \varepsilon_{gZXs} + \varepsilon_{gZXa}\\ \varepsilon_{gXYs} + \varepsilon_{gXYa} & \varepsilon_{gsY} & \varepsilon_{gYZs} - \varepsilon_{gYZa}\\ \varepsilon_{gZXs} - \varepsilon_{gZXa} & \varepsilon_{gYZs} + \varepsilon_{gYZa} & \varepsilon_{gsZ}\end{bmatrix} \tag{4.70}$$

a_{sensed} is the sensed accelerometer vector in XYZ (RPY) coordinates compensated using the prior values of compensation parameters.

ω_{sensed} is the sensed gyro vector in XYZ (RPY) coordinates compensated using the prior values of compensation parameters.

ε_{pqr} is the drift in the p sensor (accelerometer or gyroscope), q is the drift parameter (scale factor, bias or input axis misalignment), r is the drift sensor axis ($X\ or\ Y\ or\ Z$).

C_{NED}^{XYZ} is the coordinate transformation matrix from the sensor fixed coordinate frame to NED coordinate frame defined by Equation 3.17.

For gimbaled systems, the matrix C_{NED}^{XYZ} will be an identity matrix with sensor axes aligned to NED coordinats.

Equations 4.67 to 4.70 can be rearranged into a more convenient state-space form as

$$\frac{d}{dt}\boldsymbol{\zeta} = F_{NS}\varepsilon_{INSSENS} \tag{4.71}$$

$$F_{NS} = \begin{bmatrix}0_{3\times3} & 0_{3\times6} & 0_{3\times3} & 0_{3\times9}\\ C_{NED}^{XYZ} & F_{NS22} & 0_{3\times3} & 0_{3\times9}\\ 0_{3\times3} & 0_{3\times6} & C_{NED}^{XYZ} & F_{NS34}\end{bmatrix} \tag{4.72}$$

$$F_{NS22} = C_{NED}^{XYZ}\begin{bmatrix}a_X & 0 & 0 & 0 & a_Z & a_Y\\ 0 & a_Y & 0 & a_Z & 0 & a_X\\ 0 & 0 & a_Z & a_Y & a_X & 0\end{bmatrix} \tag{4.73}$$

$$F_{NS34} = C_{NED}^{XYZ}\begin{bmatrix}\omega_X & 0 & 0 & 0 & \omega_Z & \omega_Y & 0 & \omega_Z & -\omega_Y\\ 0 & \omega_Y & 0 & \omega_Z & 0 & \omega_X & -\omega_Z & 0 & \omega_X\\ 0 & 0 & \omega_Z & \omega_Y & \omega_X & 0 & \omega_Y & -\omega_X & 0\end{bmatrix} \tag{4.74}$$

Input axis alignment tends to be relatively stable, and hence initial calibration at the sensor outputs are sufficient for sensor compensation. Scale factors and biases are the usual suspects of sensor drifts. Therefore, they must be recalibrated using external sensors such as GNSS and again they should be compensated. In such cases, Equations 4.69, 4.70, 4.72, 4.73 and 4.74 can respectively be modified as,

$$[\varepsilon_{aL}] = \begin{bmatrix} \varepsilon_{asX} & 0 & 0 \\ 0 & \varepsilon_{asY} & 0 \\ 0 & 0 & \varepsilon_{asZ} \end{bmatrix} \tag{4.75}$$

$$[\varepsilon_{gL}] = \begin{bmatrix} \varepsilon_{gsX} & 0 & 0 \\ 0 & \varepsilon_{gsY} & 0 \\ 0 & 0 & \varepsilon_{gsZ} \end{bmatrix} \tag{4.76}$$

$$F_{NS} = \begin{bmatrix} 0_{3\times3} & 0_{3\times3} & 0_{3\times3} & 0_{3\times3} \\ C_{NED}^{XYZ} & F_{NS22} & 0_{3\times3} & 0_{3\times3} \\ 0_{3\times3} & 0_{3\times3} & C_{NED}^{XYZ} & F_{NS34} \end{bmatrix} \tag{4.77}$$

$$F_{NS22} = C_{NED}^{XYZ} \begin{bmatrix} a_X & 0 & 0 \\ 0 & a_Y & 0 \\ 0 & 0 & a_Z \end{bmatrix} \tag{4.78}$$

$$F_{NS34} = C_{NED}^{XYZ} \begin{bmatrix} \omega_X & 0 & 0 \\ 0 & \omega_Y & 0 \\ 0 & 0 & \omega_Z \end{bmatrix} \tag{4.79}$$

4.11.3. Augmented Dynamic Coefficient Matrix

From equation 4.54, 4.64 and 4.71, the augmented Dynamic Coefficient matrix can be written as

$$\frac{d}{dt}\begin{bmatrix} \boldsymbol{\zeta} \\ \varepsilon_{INSSENS} \end{bmatrix} = \begin{bmatrix} F_{NN} & F_{NS} \\ 0 & F_{ss} \end{bmatrix}\begin{bmatrix} \boldsymbol{\zeta} \\ \varepsilon_{INSSENS} \end{bmatrix} + \begin{bmatrix} w_{sensor}(t) \\ w_{drift}(t) \end{bmatrix} \tag{4.80}$$

The updated sensor $\varepsilon_{INSSENS}$ can be written as,

$$\varepsilon_{INSSENS} = \begin{bmatrix} x_a \\ x_g \end{bmatrix} \tag{4.81}$$

$$x_a = \begin{bmatrix} \varepsilon_{abX} \\ \varepsilon_{abY} \\ \varepsilon_{abZ} \\ \varepsilon_{asX} \\ \varepsilon_{asY} \\ \varepsilon_{asZ} \end{bmatrix} \tag{4.82}$$

$$x_g = \begin{bmatrix} \varepsilon_{gbX} \\ \varepsilon_{gbY} \\ \varepsilon_{gbZ} \\ \varepsilon_{gsX} \\ \varepsilon_{gsY} \\ \varepsilon_{gsZ} \end{bmatrix} \tag{4.83}$$

From Equation 4.80, it can be seen that the Augmented 21×21 Dynamic Coefficient Matrix is,

$$F_{NN} = \begin{bmatrix} F_{NN} & F_{NS} \\ 0 & F_{ss} \end{bmatrix} \tag{4.84}$$

And the corresponding 21×21 process noise covariance is,

$$\mathbf{Q}_{INS} = \begin{bmatrix} \mathbf{Q}_{sen\_noise} & 0 \\ 0 & \mathbf{Q}_{drift} \end{bmatrix} \tag{4.85}$$

4.12. Stationary INS Performance Analysis

To examine the performance of stationary INS, MATLAB was used with the complete Augmented Error Dynamics model and Kalman filter to analyze the performance of INS navigation model starting with zero navigation errors. The simulation time is 10 hours, and the sensor error parameters are shown in Table 4.2. Here, the errors due to sensor input axis misalignment have been neglected.

The sensor axes of the stationary INS is aligned with the NED coordinates and kept stationary. The resulting plot of RMS per axis horizontal error versus time is shown in Figure 4.9. From the plot, we can observe that there is a sharp rise in RMS horizontal errors for the first 1 hour of data but thereafter has a relatively constant slope. For this reason, the first one hour of data is usually omitted in calculating CEP rate. From the plot, we can also conclude that INS is of no use if used independently. The errors in INS will keep on accumulating due to sensor noise, drifting of calibration parameters and coupling of drift errors into navigation errors. If the performance of stationary INS is so poor, it would be even worse under dynamic conditions. Hence, INS should be fused with other systems such as GNSS for better performance, and its drifting parameters should be continuously checked.

Table 4.2: Sensor Error Parameters

Inertial Sensor Type	Sensor Error Type	Input Axis Direction	Sensor Error Symbol	RMS Variation		Correlation Time (min)
				σ	Unit	
Acceler-ometer	Bias	Roll	ε_{abX}	30	μg	15
		Pitch	ε_{abY}	30	μg	15
		Yaw	ε_{abZ}	30	μg	15

	Scale Factor	Roll	ε_{asX}	100	ppm	15
		Pitch	ε_{asY}	100	ppm	15
		Yaw	ε_{asZ}	100	ppm	15
	Noise	All	q_{acc}	10^{-3}	$\mathrm{m/s/\sqrt{s}}$	15
Gyro-scope	Bias	Roll	ε_{gbX}	0.01	deg/h	15
		Pitch	ε_{gbY}	0.01	deg/h	15
		Yaw	ε_{gbZ}	0.01	deg/h	15
	Scale Factor	Roll	ε_{gsX}	100	ppm	15
		Pitch	ε_{gsY}	100	ppm	15
		Yaw	ε_{gsZ}	100	ppm	15
	Noise	All	q_{gyro}	10^{-5}	$\mathrm{rad/s/\sqrt{s}}$	15

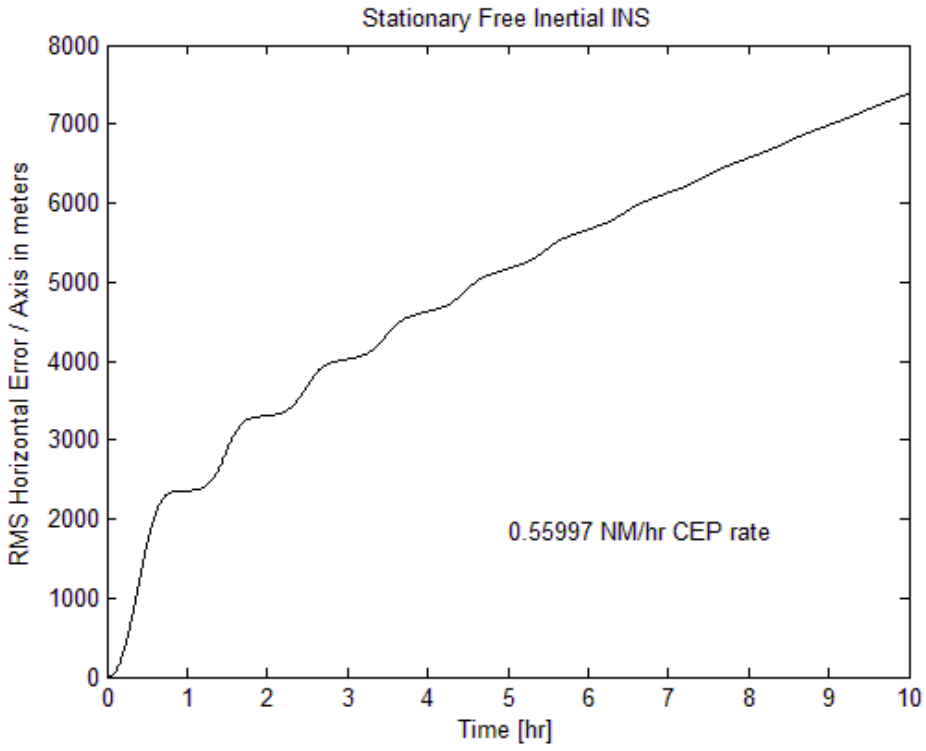

Fig 4.9: Stationary free Inertial INS Performance

Chapter 5

Global Navigation Satellite Systems (GNSS)

5.1. GNSS Systems

GNSS is a radio positioning system that uses multiple satellites to provide location and time information anywhere on or near the earth where there is an unobstructed line of sight to four or more GNSS satellites. There are currently four GNSS systems that are currently operating or are under development. These includes:

a) Global Positioning System (GPS): GPS is a satellite-based navigation system developed by U.S Department of Defense under its NAVSTAR satellite program.
b) Global Orbiting Navigation Satellite System (GLONASS): This satellite system was placed in orbit by former Soviet Union and is now maintained by the Russian Republic.
c) Galileo: The Galileo satellite system is currently under development and is being developed by the European Commission's Galileo Signal Task Force (STF) which was established in March 2001.
d) Compass (BeiDou-2): The BeiDou Navigation satellite system is being developed by the People's Republic of China (PRC). Phase I of the project was established in 2000. It became operational in China in December 2011 (Phase II) and by 2020 it would be available for global service (Phase III).

5.2. Pseudoranges

Pseudorange is the distance between a GNSS satellite and a receiver. The clocks in the satellite and the receiver are synchronized with little or no errors. Satellites send time markers as signals to the GNSS receiver. The receiver uses the time marker to calculate the travel time δt_j of the signals from the jth satellite to the receiver and use it to calculate the pseudorange between that satellite and the receiver. The pseudorange is then given by

$$\rho_j \stackrel{\text{def}}{=} c \text{ x } \delta t_j \tag{5.1}$$

$$c\ (Speed\ of\ Light) = 299{,}792{,}458\ m/s \tag{5.2}$$

GPS satellites occupy six orbital planes inclined at 55^0 from the equatorial plane. Each of the six orbital planes contain four or more satellites. The nominal satellite position in ECEF coordinates is given by Equations 3.7 to 3.12.

The pseudorange ($Z_{\rho i}$) for an ith satellite with known satellite coordinates (x_i, y_i, z_i) and unknown user coordinates (X, Y, Z) and unknown receiver clock bias (C_b) is given by

$$Z_{\rho i} = \rho^i = \sqrt{(x_i - X)^2 + (y_i - Y)^2 + (z_i - Z)^2} + C_b \tag{5.3}$$

From Equation 5.3, one can infer that at least four satellites are required (as four unknowns) to determine the receiver position given that the precise location of the satellites are known. However, if a more accurate clock receiver (expensive) is used, then three pseudoranges are suffice to know the receiver position.

5.3. GPS Signal Characteristic and Structure

GPS signals have a complex structure and hence a GPS receiver must carry out complex sequences of operations to extract useful data from the signal. Each satellite transmits two L band frequencies simultaneously denoted by L_1 (1575.42 MHz) and L_2 (1227.60 MHz). L_1 signal carrier consists of an in-phase and a quadrature-phase component. Both the components are biphase modulated by a 50 bps (bits per second) data stream. In addition, the in phase component and the quadrature phase component are modulated with a pseudorandom code called the C/A-code and the P-code respectively. In contrast, the L_2 signal is modulated by a 50 bps data stream and P-code only. The C/A or coarse/acquisition code is available to any user, military or civilian, but the P code is only available to authorized military and civilian users.

The 50 bps data stream conveys the navigation message which includes,

- Satellite Almanac Data: Almanac data or the satellite orbital data enables the user to calculate the approximate location of each and every satellite in the GPS constellation at any time. However, these data are not so accurate and can be used for initial searching of satellites when the GPS receiver is turned on.
- Satellite Ephemeris Data: Ephemeris data gives a more accurate location of satellite position. In contrast, ephemeris data is for that particular satellite that transmits the ephemeris data and the information is valid for few hours only.

- Signal Timing Data: It includes time tagging useful to calculate the pseudorange between the satellite and the user.
- Ionospheric Delay Data: There are errors introduced in the calculated pseudorange because of signal delays in the ionosphere layer of the atmosphere. These errors can be partially mitigated by using estimates of broadcasted ionospheric delay.
- Satellite Health Message: The current health of the satellite is also transmitted in the data stream so that the receiver can ignore those satellites which are not operating properly.

A complete GPS message comprises of 25 frames with each frame containing 1500 bits. Each frame is further subdivided into five 300-bit sub frames, and each sub frame comprises of 10 words of 30 bits each, with the most significant bit (MSB) of the word transmitted first. Hence, it takes 6 s to transmit a sub frame and 30 s to transmit one complete frame at the data transmission rate of 50-bps (bits per second). Transmission of the complete 25-frame navigation message takes 750 s, or 12.5 min.

5.4. Kalman Filter Implementation & Dilution of Precision (DOP)

5.4.1. Dilution of Precision (DOP)

The accuracy of position estimate of GNSS depends not only on the accuracy of GNSS receiver but also on the arrangement of satellites in space. If the satellites (reference points) are well separated in space for pseudorange measurement then the accuracy of position estimate is high. However, if the satellites are clustered together, then pseudorange measurements gives nearly equal values. In such cases, small relative errors such as clock errors or range errors is greatly increased by the geometric effect. This effect that occurs as a result of satellite geometry is called the dilution of precision (DOP).

For discrete Kalman filter, the observation matrix is given by,

$$z_k = H_k x_k + v_k \tag{5.4}$$

Where $H, z \text{ and } v$ are the vectors and matrices for the *k*th observation point in time *k*. The equation for pseudorange given in Equation 5.3 is nonlinear and hence it is linearized and approximated about some nominal solution using Taylor series to give,

$$\delta Z_\rho = H^{[1]}\,\delta\mathbf{x} + v_k \tag{5.5}$$

Measurement noise v is usually assumed to be $\mathrm{N}(0, R)$. The covariance of receiver error R is assumed to be of the same error for all the measurements.

For a four satellite system Equation 5.5 can be expanded as,

$$\begin{bmatrix}\delta Z_\rho^1\\ \delta Z_\rho^2\\ \delta Z_\rho^3\\ \delta Z_\rho^4\end{bmatrix} = \begin{bmatrix}\frac{\partial\rho_r^1}{\partial x} & \frac{\partial\rho_r^1}{\partial y} & \frac{\partial\rho_r^1}{\partial z} & 1\\ \frac{\partial\rho_r^2}{\partial x} & \frac{\partial\rho_r^2}{\partial y} & \frac{\partial\rho_r^2}{\partial z} & 1\\ \frac{\partial\rho_r^3}{\partial x} & \frac{\partial\rho_r^3}{\partial y} & \frac{\partial\rho_r^3}{\partial z} & 1\\ \frac{\partial\rho_r^4}{\partial x} & \frac{\partial\rho_r^4}{\partial y} & \frac{\partial\rho_r^4}{\partial z} & 1\end{bmatrix}\begin{bmatrix}\delta x\\ \delta y\\ \delta z\\ C_b\end{bmatrix} + \begin{bmatrix}v_\rho^1\\ v_\rho^2\\ v_\rho^3\\ v_\rho^4\end{bmatrix} \tag{5.6}$$

$$\frac{\partial\rho_r^i}{\partial x} = \frac{-(x_i - X_{nom})}{\sqrt{(x_i - X_{nom})^2 + (y_i - Y_{nom})^2 + (z_i - Z_{nom})^2}} \tag{5.7}$$

$$\frac{\partial\rho_r^i}{\partial y} = \frac{-(y_i - Y_{nom})}{\sqrt{(x_i - X_{nom})^2 + (y_i - Y_{nom})^2 + (z_i - Z_{nom})^2}} \tag{5.8}$$

$$\frac{\partial\rho_r^i}{\partial z} = \frac{-(z_i - Z_{nom})}{\sqrt{(x_i - X_{nom})^2 + (y_i - Y_{nom})^2 + (z_i - Z_{nom})^2}} \tag{5.9}$$

$i = 1,2,3,4\ (i.e\ four\ satellites)$

The calculation of Geometric Degree of Precision (GDOP) and various other DOPs such as Position Degree of Precision (PDOP), Horizontal Degree of Precision (HDOP), Vertical Degree of Precision (VDOP), Time Degree of Precision (TDOP) are then defined in terms of $H^{[1]}$ matrix as as a function of time t as,

$$D(t) = \left[H^{[1]\,T} H^{[1]}\right]^{-1} (4 \times 4\ matrix) \tag{5.10}$$

$$GDOP(t) = \sqrt{tr[D(t)]} \tag{5.11}$$

$$PDOP(t) = \sqrt{D(t)_{1,1} + D(t)_{2,2} + D(t)_{3,3}} \tag{5.12}$$

$$HDOP(t) = \sqrt{D(t)_{1,1} + D(t)_{2,2}} \tag{5.13}$$

$$VDOP(t) = \sqrt{D(t)_{3,3}} \tag{5.14}$$

$$TDOP(t) = \sqrt{D(t)_{4,4}} \tag{5.15}$$

To test the effect of satellite geometry on positioning precision, a set of five satellites was taken with initial satellite orbit parameters as follows,

Table 5.1: Initial Phasings of five satellites

Satellite No.	Ω_0 in degrees	θ_0 in degrees
1	26	340
2	146	198
3	326	68
4	86	271
5	206	90

The satellite orbits in this simulation is assumed to be of circular shape with an inclination angle of 550. The parameter Ω_0and θ_0 are the satellite "Keplerian" parameters defined in section 3.3.3. The radius of this circular orbit is 26,560,000 m and the satellites takes about 43,082 seconds (less than half a day) to complete one complete revolution around earth. In ECEF coordinate system, the equations of motion that defines the orbits of the satellites is given by the equations 3.10 and 3.11. In this simulation, two sets of satellites are taken with each set containing four satellites. For the first case, satellites 1, 2, 3, and 4 is chosen as a favorable set of satellites that results in better performance and for the second case, satellites 1, 2, 3, and 5 is chosen as an unfavorable set of satellites that results in dreaded performance.

To simplify the mathematics, the orbital frame coordinates has been transformed from the ECEF coordinate system to a locally level coordinate frame. Then, the satellite positions in local reference frame becomes

$$x_{loc} = y, \qquad y_{loc} = z, \qquad z_{loc} = x - R_e \tag{5.16}$$

where (x, y, z) are the original ECEF coordinates as defined in Equations 3.7 to 3.9, $(x_{loc}, y_{loc}, z_{loc})$ are the locally level coordinates of the satellites and R_e is the radius of the earth. To simplify the calculations, we assume that the user is situated at (0, 0, 0) coordinate in locally level reference frame. The pseudorange for the i^{th} satellite is then given by,

$$\rho^i = \sqrt{(x_i - 0)^2 + (y_i - 0)^2 + (z_i - 0)^2} \tag{5.17}$$

$$h_x^{[1]}(t) = -(x_i - 0)/\rho^i \tag{5.18}$$

$$h_y^{[1]}(t) = -(y_i - 0)/\rho^i \tag{5.19}$$

$$h_z^{[1]}(t) = -(z_i - 0)/\rho^i \tag{5.20}$$

$i = 1,2,3,4\ (i.e\ four\ satellites)$

(x_i, y_i, z_i) are the coordinates of the satellite in locally level coordinates as defined in Equation 5.16.

5.4.2. Kalman Filter Implementation

Kalman filter is used here for a couple of applications. First, it is used to demonstrate how the filter converges the errors to its minimum error bound. Second, the Kalman filter is used to test the performance of GPS system as a function of different satellite geometry. The convergence of the system is checked by performing a covariance analysis on the GPS system, given initial error estimates $\mathbf{P_0}(+)$, the initial transformation matrix ϕ , the initial measurement covariance matrix $\mathbf{R}$ and the initial process covariance matrix $\mathbf{Q}$. The values of these matrices that are used in the implementation are as follows,

$$\mathbf{Q} = \begin{bmatrix} 0.333 & 0 & 0 & 0 & 0 \\ 0 & 0.333 & 0 & 0 & 0 \\ 0 & 0 & 0.333 & 0 & 0 \\ 0 & 0 & 0 & 0.0833 & 0 \\ 0 & 0 & 0 & 0 & 0.142 \end{bmatrix} \tag{5.21}$$

$$\mathbf{R} = \begin{bmatrix} 225 & 0 & 0 & 0 \\ 0 & 225 & 0 & 0 \\ 0 & 0 & 225 & 0 \\ 0 & 0 & 0 & 225 \end{bmatrix} \tag{5.22}$$

$$\phi = \begin{bmatrix} 1 & 0 & 0 & 0 & 0 \\ 0 & 1 & 0 & 0 & 0 \\ 0 & 0 & 1 & 0 & 0 \\ 0 & 0 & 0 & 1 & 1 \\ 0 & 0 & 0 & 0 & 1 \end{bmatrix} \tag{5.23}$$

$$\mathbf{P_0}(+) = \begin{bmatrix} 10{,}000 & 0 & 0 & 0 & 0 \\ 0 & 10{,}000 & 0 & 0 & 0 \\ 0 & 0 & 10{,}000 & 0 & 0 \\ 0 & 0 & 0 & 90{,}000 & 0 \\ 0 & 0 & 0 & 0 & 900 \end{bmatrix} \tag{5.24}$$

Here, it is assumed that the clock bias error is 300m and drift is 30 m/s. The discrete extended Kalman filtering equations can be written as,

A priori covariance matrix

$$\mathbf{P_k}(-) = \boldsymbol{\phi}\mathbf{P_{k-1}}(+)\boldsymbol{\phi}^{\mathbf{T}} + \mathbf{Q_{k-1}} \tag{5.25}$$

Kalman gain equation

$$\bar{\mathbf{K}}_{\mathbf{k}} = \mathbf{P_k}(-)\mathbf{H_k^T}\left[\mathbf{H_k}\mathbf{P_k}(-)\mathbf{H_k^T} + \mathbf{R_k}\right]^{-1} \tag{5.26}$$

A posteriori covariance matrix

$$\mathbf{P_k}(+) = \{\mathbf{I} - \bar{\mathbf{K}}_\mathbf{k}\mathbf{H_k}\}\mathbf{P_k}(-) \quad (5.27)$$

In this simulation, the matrices $\mathbf{Q}$, $\mathbf{R}$ and ϕ comes out to be a satisfactory set of initial covariance estimates. This type of analysis is generally done when the actual data are not available but this analysis can give an estimate of how well the system will converge. However, the matrices $\mathbf{Q}$, $\mathbf{R}$ and ϕ in a real system are under the control of the designer. These matrices should be carefully designed to get an acceptable residual covariance error.

5.4.3. DOP Calculations

The effect of satellite geometry on performance is here explained with the help of a simulation. The Kalman filter is implemented with the initial values as described in Equation 5.21 to 5.24. For the first case, satellites 1, 2, 3, and 4 is chosen as a favorable set of satellites that results in better performance and for the second case, satellites 1, 2, 3, and 5 is chosen as an unfavorable set of satellites that results in dreaded performance. After the satellites are chosen, the orbits of each of the satellites was defined using the Equations 3.10 and 3.11. The coordinates of satellite in locally level coordinates can be calculated using Equation 5.16. The sensitivity matrix elements defined in Equations 5.17 to 5.20 was calculated for each satellite and for each time instant and then the values were substituted in Equation 5.6 to get the complete sensitivity matrix. The GDOP values were calculated for the two cases. The simulation time was set for one hour and the results are as described below.

Case 1: For case 1 satellites 1, 2, 3 and 4 are chosen. The results show an excellent GDOP. Figure 5.1 shows the plot of GDOP in meters versus time in seconds. It can be inferred that the satellites are well separated in space and forms a good geometry.

Case 2: For case 2 satellites 1, 2, 3 and 5 satellites are chosen. The results shows a dreaded GDOP “chimney peak”. This peak is observed when two or more satellites are close to each other and therefore it is unable to provide a good estimate of user position. Figure 5.2 shows the plot of GDOP in meters versus time in seconds. It can be concluded that this combination of satellites cannot be used to find the user position or clock biases.

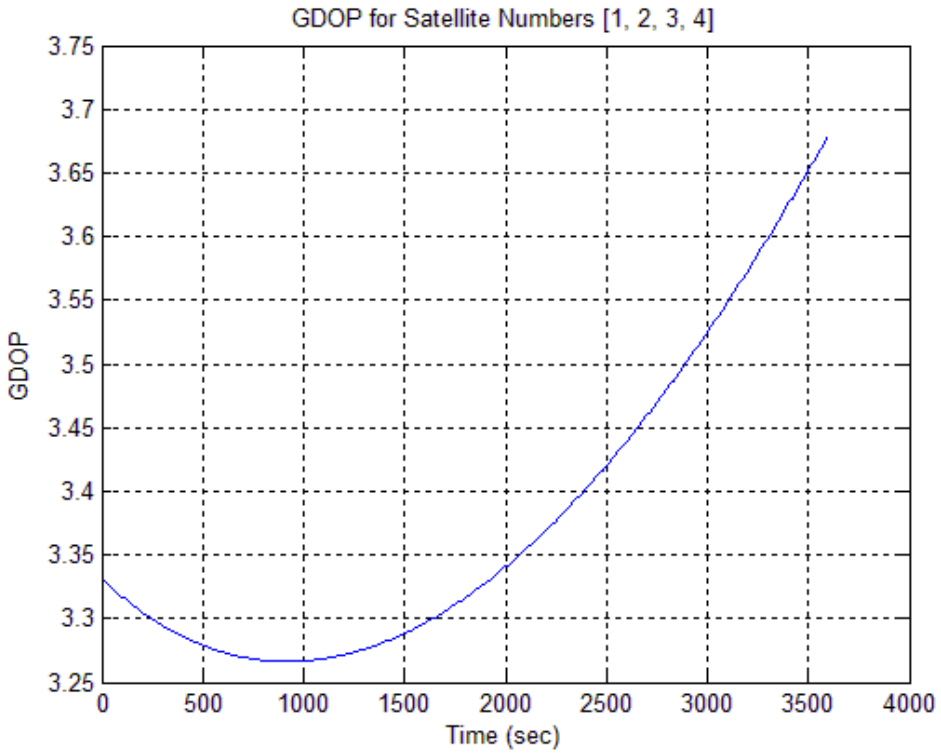

Fig 5.1: Case 1 GDOP

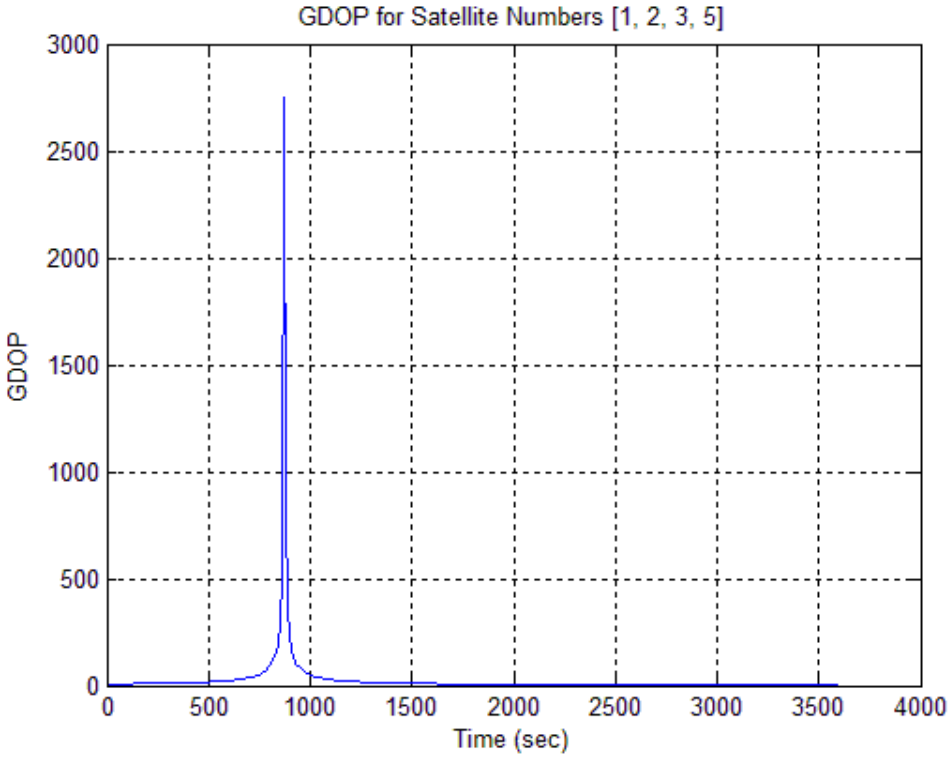

Fig 5.2: Case 2 GDOP

5.4.4. Covariance Analysis

From the Kalman filter data used in the above simulation and following the same procedure, the diagonal elements of the covariance matrices $\mathbf{P}_k(-)$ (predicted) and $\mathbf{P}_k(+)$ (corrected) are plotted as an estimate of how well the individual x, y, z and clock bias errors converge as a function of time. From the plots of Figure 5.3 to 5.6, it can be seen that the results are satisfactory.

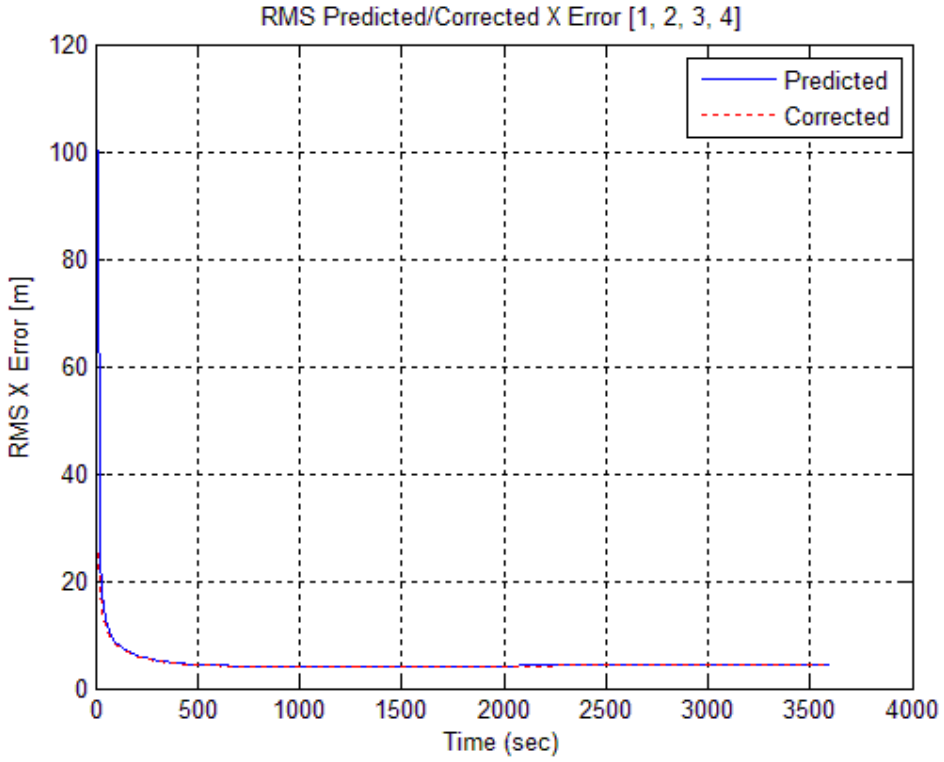

Fig 5.3: RMS East Position Uncertainties

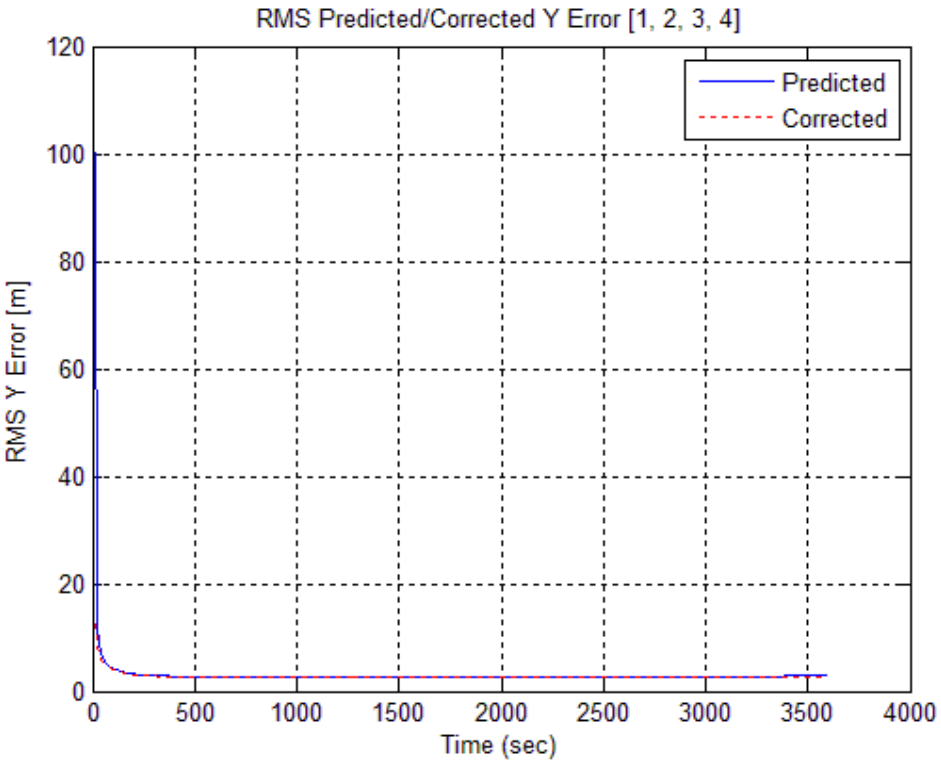

Fig 5.4: RMS North Position Uncertainties

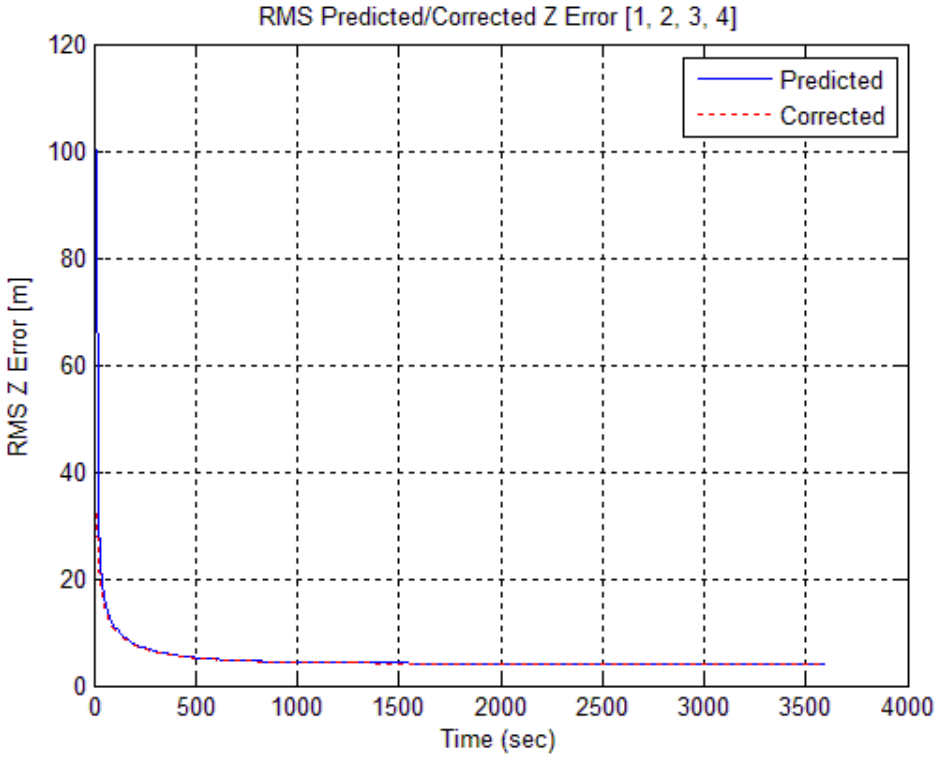

Fig 5.5: RMS Vertical Position Uncertainties

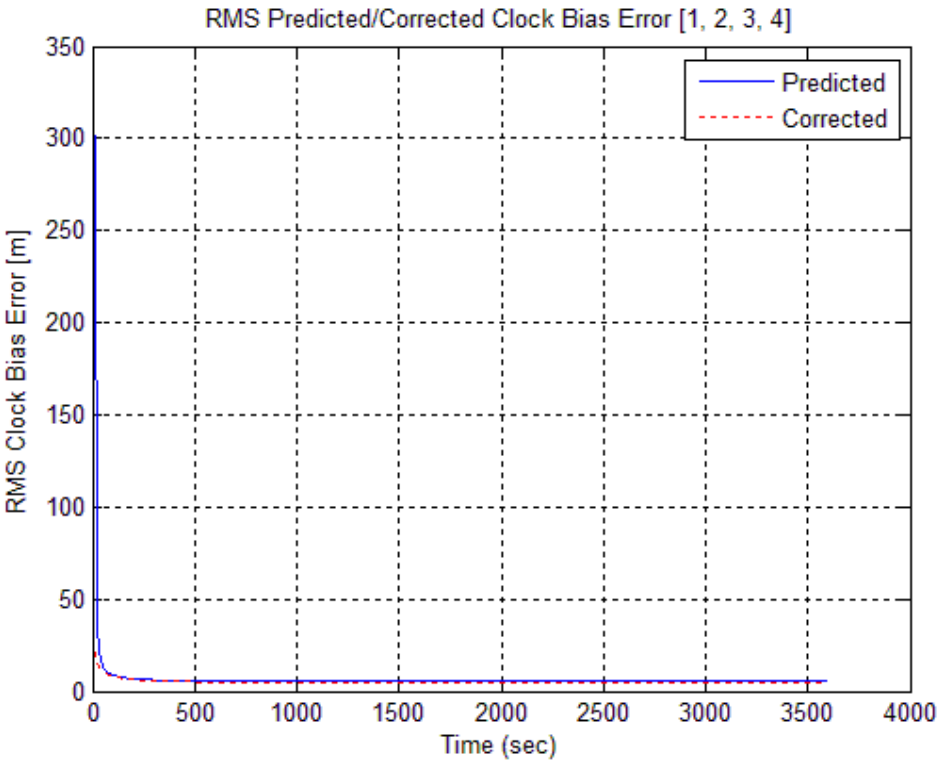

Fig 5.6: RMS Clock Bias Uncertainties

5.5. Host Vehicle Tracking Filters for GNSS

5.5.1. Dynamic Dilution of Information

"Dilution of information" refers to the reduction in accuracy of the GNSS receiver position when there is an increase in host vehicle dynamic activity. Consider a vehicle kept at standstill. During this condition, the accuracy of the estimated position of the vehicle will improve as the number of measurements for the same position are available for multiple times. However, during vehicle dynamic conditions, the most recent measurement can only be used to estimate the vehicle position. Hence, the accuracy of estimated position decreases as there is an increase in degree of dynamic motion. As GNSS receiver is a position estimator, vehicle dynamic model with higher derivatives of position must be used along with the receiver to predict unknown vehicle dynamics. As a result, with increase in number of state variables of the vehicle dynamic model, the accuracy of the estimated position should decrease. But there is another major factor that affects the accuracy of the GNSS receiver i.e. the degree to which model bounds the solution. Thus, there is a tradeoff between these two factors and the accuracy depends on the factor that is more pronounced.

Design of Kalman filter essentially requires modelling of two matrices:

1. The dynamic coefficient matrix F.

2. The process covariance matrix $\mathbf{Q}$.

Table 5.2 lists the matrix parameters that are used for designing the host vehicle dynamic model. These models are named as TYPE2, DAMP2 and DAMP3. The table also specifies the various dependent and independent parameters of the corresponding models. As all the matrix parameters are time-invariant, the finite dependent parameters can be easily obtained from the solution of steady state Ricatti differential equation. The independent parameters are usually designed by the filter designer. Table 5.3 provides the definitions of the various statistical parameters that are used in Table 5.2.

Table 5.2: Host Vehicle Dynamic Models for GNSS Receivers

Model Name	Matrix Parameters (Each Axis)		Independent Parameters	Dependent Parameters
	$\mathbf{F}$	$\mathbf{Q}$		
TYPE2	$\begin{bmatrix} 0 & 1 \\ 0 & 0 \end{bmatrix}$	$\begin{bmatrix} 0 & 0 \\ 0 & \sigma_{acc}^2 \Delta t^2 \end{bmatrix}$	σ_{acc}^2	$\sigma_{pos}^2 \longrightarrow \infty$ $\sigma_{vel}^2 \longrightarrow \infty$
DAMP2	$\begin{bmatrix} 0 & 1 & 0 \\ 0 & \frac{-1}{\tau_{vel}} & 1 \\ 0 & 0 & \frac{-1}{\tau_{acc}} \end{bmatrix}$	$\begin{bmatrix} 0 & 0 & 0 \\ 0 & 0 & 0 \\ 0 & 0 & \sigma_{jerk}^2 \Delta t^2 \end{bmatrix}$	σ_{vel}^2 σ_{acc}^2 τ_{acc}	$\sigma_{pos}^2 \longrightarrow \infty$ τ_{vel} $\rho_{vel,acc}$ σ_{jerk}^2
DAMP3	$\begin{bmatrix} \frac{-1}{\tau_{pos}} & 1 & 0 \\ 0 & \frac{-1}{\tau_{vel}} & 1 \\ 0 & 0 & \frac{-1}{\tau_{acc}} \end{bmatrix}$	$\begin{bmatrix} 0 & 0 & 0 \\ 0 & 0 & 0 \\ 0 & 0 & \sigma_{jerk}^2 \Delta t^2 \end{bmatrix}$	σ_{pos}^2 σ_{vel}^2 σ_{acc}^2 τ_{acc}	τ_{pos} τ_{vel} $\rho_{pos,vel}$ $\rho_{pos,acc}$ $\rho_{vel,acc}$ σ_{jerk}^2

Table 5.3: Host Vehicle Model Statistical Parameters

Symbol	Definition
σ_{pos}^2	$E(\|p\|^2)$, Mean squared position of vehicle
σ_{vel}^2	$E(\|v\|^2)$, Mean squared velocity of vehicle
σ_{acc}^2	$E(\|a\|^2)$, Mean squared acceleration of vehicle
σ_{jerk}^2	$E(\|\dot{a}\|^2)$, Mean squared jerk
$\rho_{i,j}$	Correlation coefficients between variations of accelerations, velocity and position.
τ_{pos}	Position correlation time
τ_{vel}	Velocity correlation time
τ_{acc}	Acceleration correlation time

5.5.2. Figure 8 Tracking Model

To implement and observe the effects of Host vehicle dynamics Models on the accuracy of GNSS receivers, a track has to be designed on which the models can be tested. We will use a three dimensional figure-8 track for this purpose.

The trajectory of the track in NED coordinates is defined as given below,

$$\delta_{pos} = \begin{bmatrix} Northing \\ Easting \\ -Altitude \end{bmatrix} = \begin{bmatrix} 3\,S\sin(\omega t + \phi) \\ 2\,S\sin(\omega t + \phi)\cos(\omega t + \phi) \\ -1/2\ \mathrm{h}\cos(\omega t + \phi) \end{bmatrix} \tag{5.28}$$

where S is a track scaling parameter, [track length in meters]/14.94375529901562, h is half the vertical separation where the track crosses over itself, ω = 2π ×[average speed (m/s)]/[track length (m)], and ϕ is an arbitrary phase angle (rad).

The model is implemented in MATLAB and the output is shown in Figure 5.7. To completely represent the Dynamic model parameters, various other statistical parameters are required as shown in Table 5.3. MATLAB was used to calculate the required parameters on Figure 8 track. Figure 5.8 to 5.10 shows the autocorrelation functions for position, velocity and acceleration for Figure-8 Track. The correlation time constant for position, velocity and acceleration is calculated using the autocorrelation function.

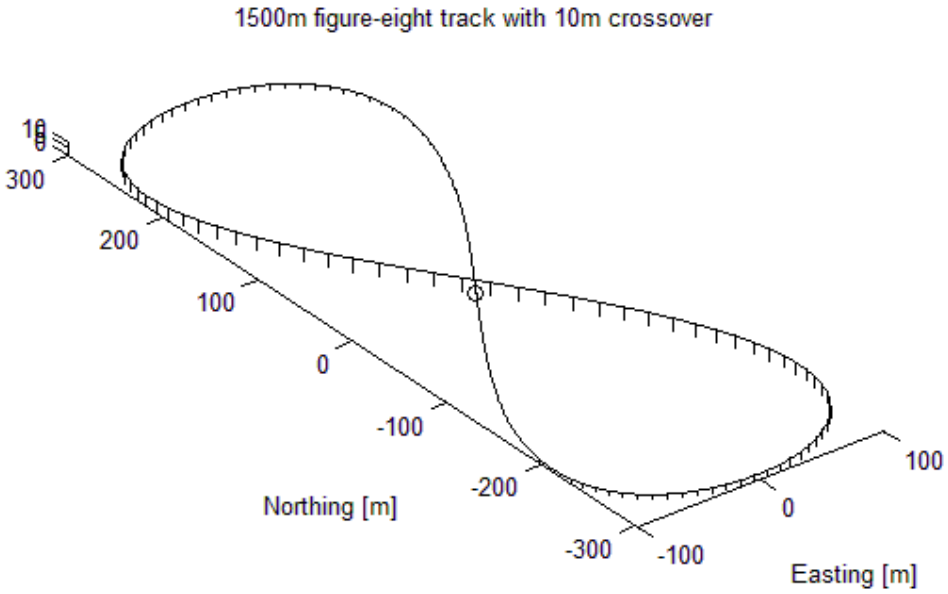

Fig 5.7: Figure-8 Trajectory

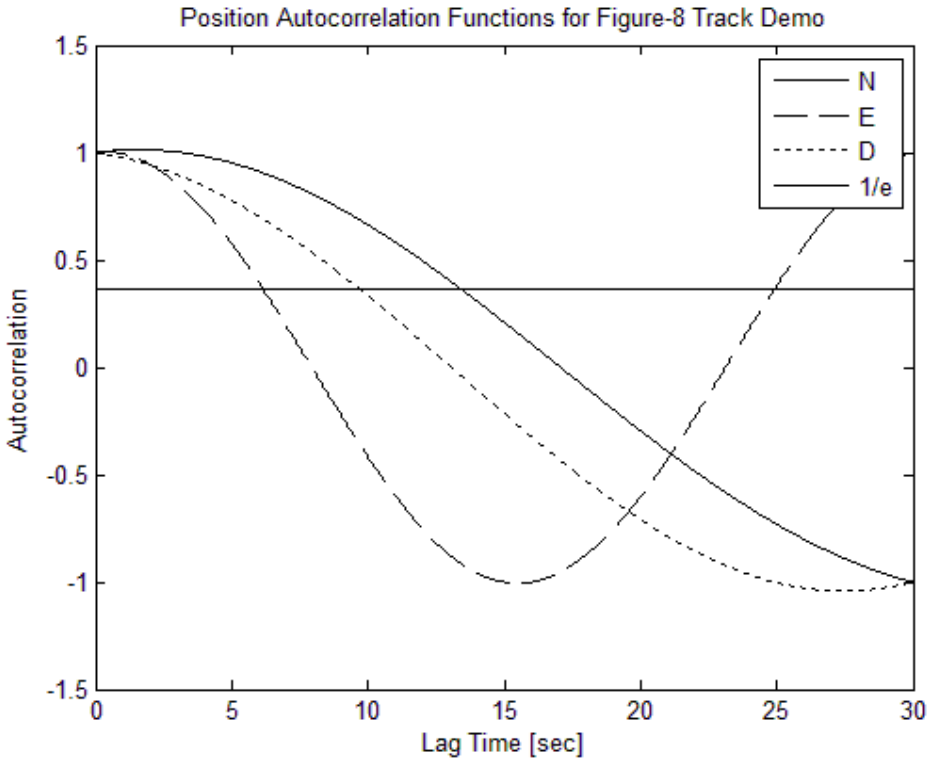

Fig 5.8: Position autocorrelation function

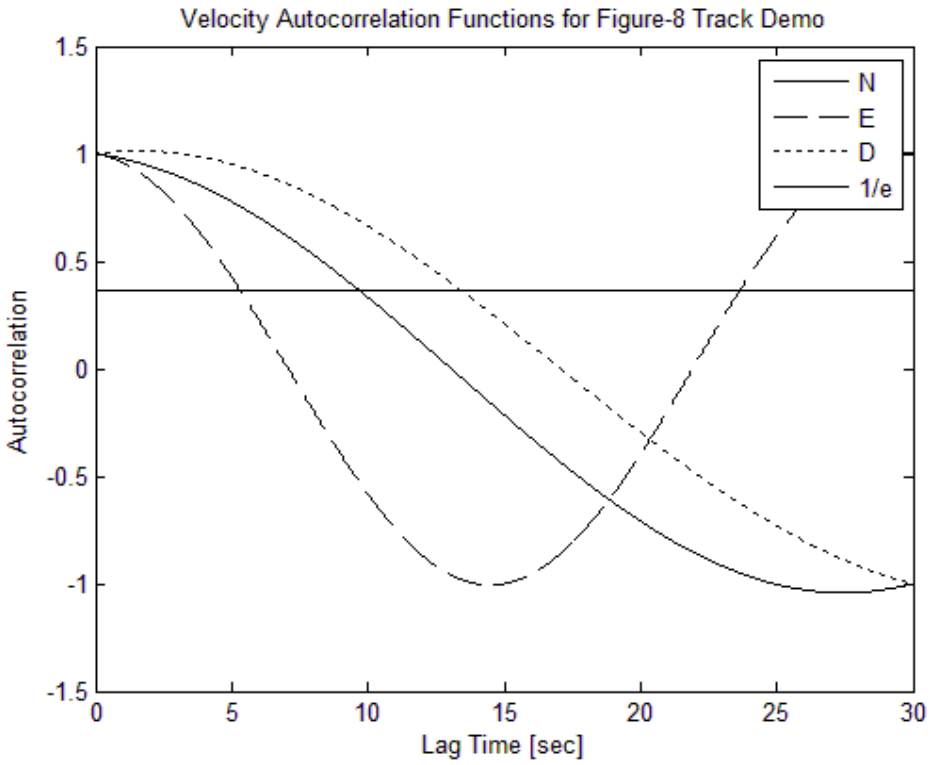

Fig 5.9: Velocity autocorrelation function

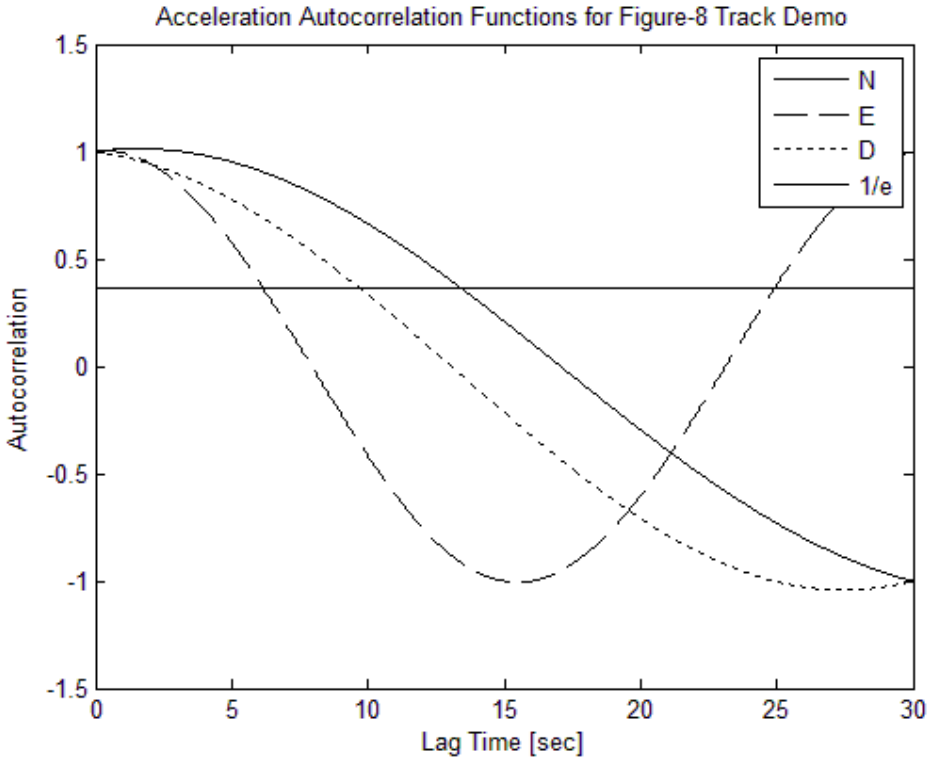

Fig 5.10: Acceleration autocorrelation function

The output statistical parameters are as follows:

RMS N-S Position = 212.9304 meter
RMS E-W Position = 70.9768 meter
RMS Vert. Position = 3.5361 meter
RMS N-S Velocity = 22.3017 m/s
RMS E-W Velocity = 14.8678 m/s
RMS Vert. Velocity = 0.37024 m/s
RMS N-S Acceleration = 2.335 m/s/s
RMS E-W Acceleration = 3.1134 m/s/s
RMS Vert. Acceleration = 0.038778 m/s/s
RMS Delta Velocity North = 0.02335 m/s at Delta t = 0.01 sec.
RMS Delta Velocity East = 0.031134 m/s at Delta t = 0.01 sec.
RMS Delta Velocity Down = 0.00038771 m/s at Delta t = 0.01 sec.
N. Position Correlation Time = 13.4097 sec
E. Position Correlation Time = 7.6696 sec
Vertical Position Corr. Time = 9.6786 sec
N. Velocity Correlation Time = 9.6786 sec
E. Velocity Correlation Time = 21.4921 sec
Vertical Velocity Corr. Time = 13.4097 sec
N. Acceler. Correlation Time = 13.4097 sec
E. Acceler. Correlation Time = 7.6696 sec
Vertical Acceler. Corr. Time = 9.6786 sec

5.5.3. GNSS Filter Comparison

The comparison of various GNSS Dynamic model was done with the help of MATLAB. Using the statistical parameter obtained from the analysis of Figure 8 Track, the model parameters was constructed for each axis using Table 5.2. Then the individual axis model was augmented to give a three axis model parameters. The host vehicle model was further augmented with the propagation delay model described in Section 5.6.2. The process was repeated for all the three models namely TYPE2, DAMP2 and DAMP3 to give the dynamic coefficient matrix **F** and the dynamic disturbance covariance matrix **Q.** The output is as shown in Figure 5.11 and Table 5.4 shows the comparison of GNSS filters on 1.5 km Figure-8 Track.

For the simulation, 29 satellites were used with initial right ascension angle (Ω_0) data and initial angular location (θ_0) data of the satellite taken from www.navcen.uscg.gov. The orbits are assumed to be circular and move along the trajectory defined by Equations 3.7 to 3.11 in ECEF coordinates. In the simulation, it is assumed that the satellites that are not 15 degrees above the horizon are not detectable. Hence their sensitivities are zeroed out. The number of satellites that are available during the simulation with these settings are plotted in Figure 5.12. From the results, it could be seen that the number of satellites that are available at any time instant during the simulation lies between 9 and 11.

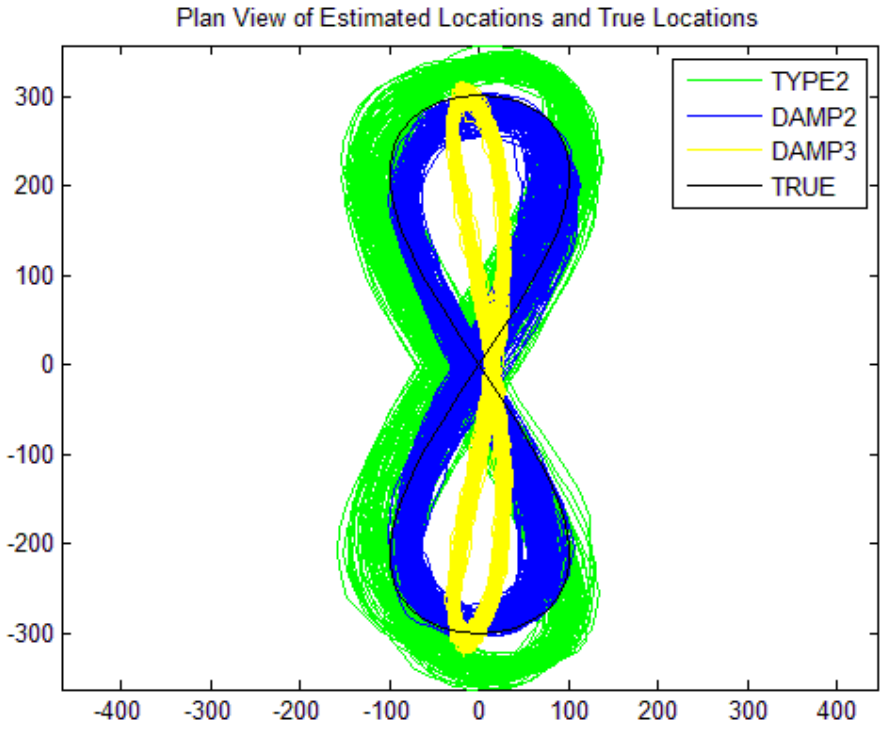

Fig 5.11: Comparison of GNSS Filters

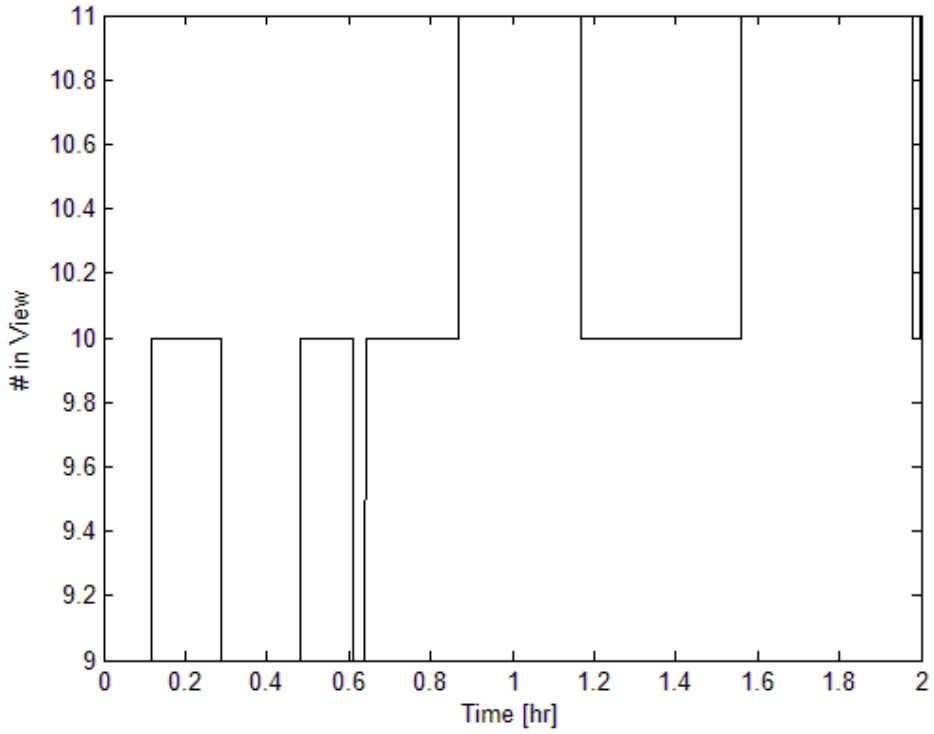

Fig 5.12: Number of satellites in View

Table 5.4: Comparison of GNSS Filters on Figure-8 Track

GNSS Filter	RMS Position Estimated Errors (m)		
	North	East	Down
TYPE2	42.0705	41.0979	4.6252
DAMP2	23.1501	25.279	3.5128
DAMP3	7.996	11.3024	3.1534

From the results of Table 5.4, it could be seen that DAMP3 model is most suited for the GNSS receiver under dynamic conditions even though DAMP3 models uses three more state variables than do DAMP2 or TYPE2 models. This is because DAMP3 filter constrains the solution of the system and the effect due to dilution of information is not so much pronounced. Hence, the simulated performance improves down the table and is best for DAMP3.

5.6. GNSS Error Models

Apart from the unpredictable motions of the host vehicle that results in dilution of information of measured pseudoranges, there are other sources of error such as GNSS clock receiver errors, signal propagation delay errors and pseudorange measurement noise that influences the accuracy of the estimates of position and velocity in the GNSS receiver. Three or four pseudorange measurements are enough for determining receiver's position but the receiver can use about a dozen pseudorange to estimate position. The Kalman filter can use the redundant data to remove the effect of error sources in the overall system. The various errors and their models are described in this section. Another conclusion that can be made from the Figure 5.11 is that GNSS performance does not degrade with time as it is in the case of INS.

5.6.1. Clock Error Models

The clocks used in GNSS satellites are highly accurate clocks. GNSS receiver clocks are quite stable over a period of 10s. The receiver use timing information from clocks of GNSS satellites to maintain long-term accuracy and stability of their own clocks. The timing information is updated in receivers at an interval of 1s. The receiver can then track their own clock errors relatively accurately. To keep the receiver clock synchronized with the GNSS satellite clock, Kalman filter is used with two state variables. This tracker is also called as the type 2 tracker. GNSS receiver clock model state variables are,

a) $\varepsilon_{clock\ bias}$, clock bias in meters

b) $\varepsilon_{clock\ drift}$, clock drift rate in meters per second

The clock drift model are generally exponentially correlated

$$\frac{d}{dt}\varepsilon_{clock\ drift} = \frac{-1}{\tau_{clock\ drift}}\varepsilon_{clock\ drift} + w_{clock\ drift}(t) \tag{5.29}$$

$$\frac{d}{dt}\varepsilon_{clock\ bias} = \varepsilon_{clock\ drift} \tag{5.30}$$

The dynamic model has the form,

$$\frac{d}{dt}\begin{bmatrix}\varepsilon_{clock\ bias}\\ \varepsilon_{clock\ drift}\end{bmatrix} = \begin{bmatrix}0 & 1\\ 0 & \frac{-1}{\tau_{clock\ drift}}\end{bmatrix}\begin{bmatrix}\varepsilon_{clock\ bias}\\ \varepsilon_{clock\ drift}\end{bmatrix} + \begin{bmatrix}0\\ w_{clock\ drift}(t)\end{bmatrix} \tag{5.31}$$

$$F_{clock} = \begin{bmatrix} 0 & 1 \\ 0 & \dfrac{-1}{\tau_{clock\ drift}} \end{bmatrix} \tag{5.32}$$

The noise covariance can be written as,

$$q_{clock\ drift} = E\left(w^2_{clock\ drift}(t)\right) = \frac{2\sigma^2_{clock\ drift}}{\tau_{clock\ drift}} \tag{5.33}$$

$$\mathbf{Q}_{clock} = \begin{bmatrix} 0 & 0 \\ 0 & \dfrac{2\sigma^2_{clock\ drift}}{\tau_{clock\ drift}} \end{bmatrix} \tag{5.34}$$

Where $\sigma^2_{clock\ drift}$ is the steady state variance of clock drift.

5.6.2. Atmospheric Propagation Delay Model

As the GNSS signals pass through the atmosphere to reach the receiver, there is small decrease in the speed of light in the ionosphere layer of the atmosphere. This delay is quite unpredictable and hence it introduces unpredictable errors in the estimated pseudoranges. Propagation delays are modeled as independent, exponentially correlated errors. The dimensions of the dynamic coefficient matrix and process noise covariance matrix are of the same dimensions as the number of satellites available.

$$F_{sat\_delay} = \frac{-1}{\tau_{sat\_delay}} \begin{bmatrix} 1 & 0 & 0 & \cdots & 0 \\ 0 & 1 & 0 & \cdots & 0 \\ 0 & 0 & 1 & \cdots & 0 \\ \vdots & \vdots & \vdots & \ddots & \vdots \\ 0 & 0 & 0 & \cdots & 1 \end{bmatrix} \tag{5.35}$$

$$\mathbf{Q}_{sat\_delay} = q_{sat\_delay} \begin{bmatrix} 1 & 0 & 0 & \cdots & 0 \\ 0 & 1 & 0 & \cdots & 0 \\ 0 & 0 & 1 & \cdots & 0 \\ \vdots & \vdots & \vdots & \ddots & \vdots \\ 0 & 0 & 0 & \cdots & 1 \end{bmatrix} \tag{5.36}$$

5.6.3. Pseudorange Measurement Noise

There are some errors introduced at the time of the measurement of pseudorange distance in the GNSS receivers. These errors are due to additive electronic noise and signal processing noise. These errors are modeled as measurement noise covariance matrix. The measured pseudorange from k satellites at the same time epoch can be written as,

$$z = \begin{bmatrix} \rho_1 \\ \rho_2 \\ \rho_3 \\ \vdots \\ \rho_k \end{bmatrix} + \begin{bmatrix} v_1 \\ v_2 \\ v_3 \\ \vdots \\ v_k \end{bmatrix} \tag{5.37}$$

where ρ_k is the true pseudorange from the k^{th} satellite and v_k is the added zero mean white noise with variance of σ^2. The additive noise are correlated over time (generally removed by filtering) but uncorrelated between satellites. The measurement noise covariance can then be written as,

$$R_{pseudo} = E\left\langle \begin{bmatrix} v_1 \\ v_2 \\ v_3 \\ \vdots \\ v_k \end{bmatrix} [v_1 \quad v_2 \quad v_3 \quad \dots \quad v_k] \right\rangle \tag{5.38}$$

$$= \begin{bmatrix} \sigma^2 & 0 & 0 & \cdots & 0 \\ 0 & \sigma^2 & 0 & \cdots & 0 \\ 0 & 0 & \sigma^2 & \cdots & 0 \\ \vdots & \vdots & \vdots & \ddots & \vdots \\ 0 & 0 & 0 & \cdots & \sigma^2 \end{bmatrix} \tag{5.39}$$

The models developed in this chapter shall be used for integrating GNSS with INS and analyzing their performance in the next chapter of the thesis.

Chapter 6

GNSS/INS Sensor Fusion

6.1. Benefits of GNSS/INS Fusion

Sensor Fusion or Sensor Integration is the process of combining two or more sensory data derived from disparate sources such that the resulting system has better performance than the performance of each system when operated individually. One of the earliest implementation of GNSS/INS integration was to stabilize the altitude estimates of an INS which are otherwise unstable. This methodology was soon expanded to be used in the horizontal components of INS position and velocity to correct horizontal errors. The integration of GNSS and INS in positioning has several benefits such as,

- The integrated system can be operated even with sensors with lower performance. Hence, the overall cost of the system is reduced.
- The errors in INS keeps on accumulating and after few hours it becomes useless. GNSS aids INS to track the drifting parameter of the INS errors so that the INS performance does not degrade with time when GNSS is available.
- In an integrated system, an INS is allowed to navigate with improved initial error whenever the GNSS signals are unavailable.
- The GNSS receiver now no longer requires a stochastic model for the host vehicle dynamics. The integrated system measures the host vehicle dynamics directly.
- INS aids GNSS by improving signal reacquisition time and also by reducing signal phase tracking lags in the GNSS receiver whenever the GNSS signals becomes available again.

6.2. Integration Ranking

The integration algorithms are ranked according to the level of coupling between the inertial navigators and GNSS receivers. The rankings are generally called as loosely coupled, tightly coupled and ultratightly coupled integration. Although, the ranking does provides some information on what is involved in different levels of integration, it is not always possible to

say whether one implementation is strictly looser or tighter as there are many levels of implementation.

6.2.1. *Loosely coupled Integration*: In this type of implementation, the navigation solution from GNSS and INS are treated independently and their outputs are combined with the help of a Kalman filter. The down side of this type of approach is that neither GNSS nor INS is made any better. Over time, the estimate of an INS gets worse and hence its filter weighing gets smaller. Eventually, the navigation solution is due to GNSS only and the INS solution is ignored. When GNSS signals are lost, the INS navigation solution is of no use.

6.2.2. *Tightly Coupled Integration*: This type of implementation alters the internal working of the GNSS receiver and INS and overall performance of the system is improved. Raw pseudoranges and raw accelerations from the GNSS receiver and the accelerometer respectively may independently produce their own navigation solution. All data produced are made available for the unified navigation solution. The unified filter model must include variables such as accelerometer bias errors, scale factor errors, signal propagation delays, etc. The estimated values of these variables are used in the internal implementation of INS and GNSS receiver. This thesis presents the unified model for tightly coupled integration in further parts of this chapter.

6.2.3. *Ultratightly Coupled Integration*: In this type of implementation, signal tracking loops in the GNSS receiver are augmented by using accelerations and rotations sensed by the INS. This is mainly done to improve phase locking and reduce phase tracking filter lags during high maneuvering periods or reduced signal strength. GNSS signal reacquisition time is also improved by this approach. However, models for this type of integration are not developed in this thesis. This approach using Kalman filtering has been discussed in [13].

6.3. Unified GNSS/INS Error Model

Individual models for GNSS and INS has been developed in previous chapters. This section mainly deals with development of unified model for integration of GNSS and INS and analyzing the performance of the model using Kalman Filtering. For designing a Kalman filter, Dynamic

Coefficient matrix (F_{Fused}), Process noise covariance matrix ($\mathbf{Q}_{Fused}$) and Measurement sensitivity matrix (H_{Fused}) needs to be defined.

6.3.1. Dynamic Coefficient Matrix

The matrix structure for the dynamic coefficient matrix can be written as,

$$F_{Fused} = \begin{bmatrix} F_{NN} & F_{NS} & 0 & 0 \\ 0 & F_{ss} & 0 & 0 \\ 0 & 0 & F_{clock} & 0 \\ 0 & 0 & 0 & F_{sat\_delay} \end{bmatrix} \tag{6.1}$$

F_{NN} is the 9×9 dynamic coefficient matrix for INS navigation errors as defined by Equation 4.36.

F_{NS} is the 9×12 dynamic coupling matrix as defined by Equation 4.77.

F_{ss} is the 12×12 dynamic coefficient matrix for the twelve sensor compensation parameters as defined by equation 4.65.

F_{clock} is the 2×2 dynamic coefficient matrix for GNSS receiver clock errors as defined by Equation 5.32.

F_{sat_delay} is the 31×31 dynamic coefficient matrix for propagation delay errors as defined by Equation 5.35.

The number of satellites used in this model is 31. The number of state variables adds up to $9 + 12 + 2 + 31 = 54$. Therefore, the dimensions of the dynamic coefficient matrix for the unified model is 54×54.

6.3.2. Process Noise Covariance Matrix

The sources of process noise in the integrated system are from inertial sensors, drifting compensation parameters, GNSS receiver clock and atmospheric signal delays. The matrix structure for process noise covariance can be modeled as,

$$\mathbf{Q}_{Fused} = \begin{bmatrix} \mathbf{Q}_{sen\_noise} & 0 & 0 & 0 \\ 0 & \mathbf{Q}_{drift} & 0 & 0 \\ 0 & 0 & \mathbf{Q}_{clock} & 0 \\ 0 & 0 & 0 & \mathbf{Q}_{sat\_delay} \end{bmatrix} \tag{6.2}$$

$\mathbf{Q}_{sen\_noise}$ is the 9×9 process noise covariance matrix for INS navigation errors as defined by Equation 4.54.

$\mathbf{Q}_{drift}$ is the 12×12 process noise covariance matrix for the twelve sensor compensation parameters as defined by equation 4.66.

$\mathbf{Q}_{clock}$ is the 2×2 process noise covariance matrix for GNSS receiver clock errors as defined by Equation 5.34.

$\mathbf{Q}_{sat\_delay}$ is the 31×31 process noise covariance matrix for propagation delay errors as defined by Equation 5.36.

6.3.3. Measurement Sensitivity Matrix

The pseudorange measurement sensitivity is represented in terms of a unit vector from the antenna of the satellite to the antenna of the receiver. The sensitivity matrix for the i^{th} satellite will have the structure,

$$H_i = [a_{iN} \quad a_{iN} \quad a_{iD} \quad 0 \quad 0 \quad \cdots \quad 0 \quad 1 \quad 0 \quad \cdots \quad 0 \quad 1 \quad 0 \quad \cdots] \tag{6.3}$$

where

$$\mathbf{a}_i = [a_{iN} \quad a_{iN} \quad a_{iD}]^T \tag{6.4}$$

is a unit vector from the satellite to the receiver.

The first 'one' comes in the 22nd position which is the sensitivity due to clock bias and the final 'one' comes in the $(23 + i)^{th}$ position which is due to propagation delay for the i^{th} satellite.

6.4. GNSS/INS Simulation Results

The unified model developed in Section 6.3 is tested on a figure-8 track of 1500m. The simulation time is set at 6 hours and after one hour of operation, the GNSS measurement is halted for one hour. The performance of the unified model is observed under both cases, that is when the GNSS signal is lost and again when GNSS signals are reacquired. The model use a cluster of 31 satellites to provide pseudorange measurement to the GNSS receiver. The performance of other error parameters such as positon uncertainty, velocity uncertainty, sensor drifts, clock biases and pseudrange delay is also analyzed. Out of the 31 satellites used in the simulation, the satellites that are not 15 degrees above the horizon are ignored assuming that these satellites are not visible to the GNSS receiver. The MATLAB simulation results for the above results are as shown below,

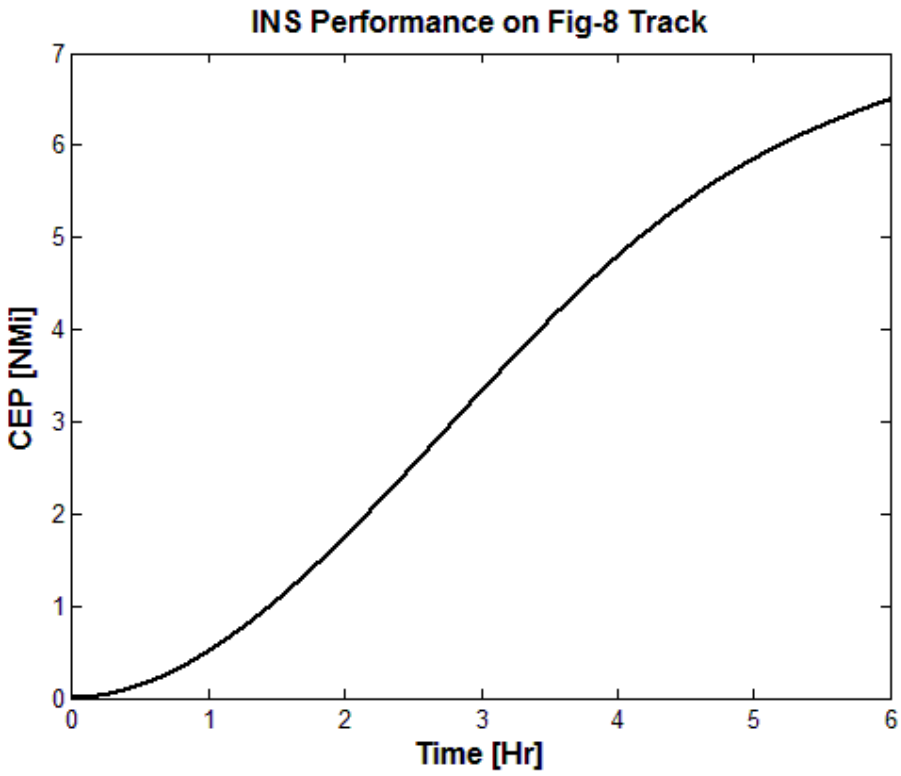

Fig 6.1: INS Performance on Fig-8 Track

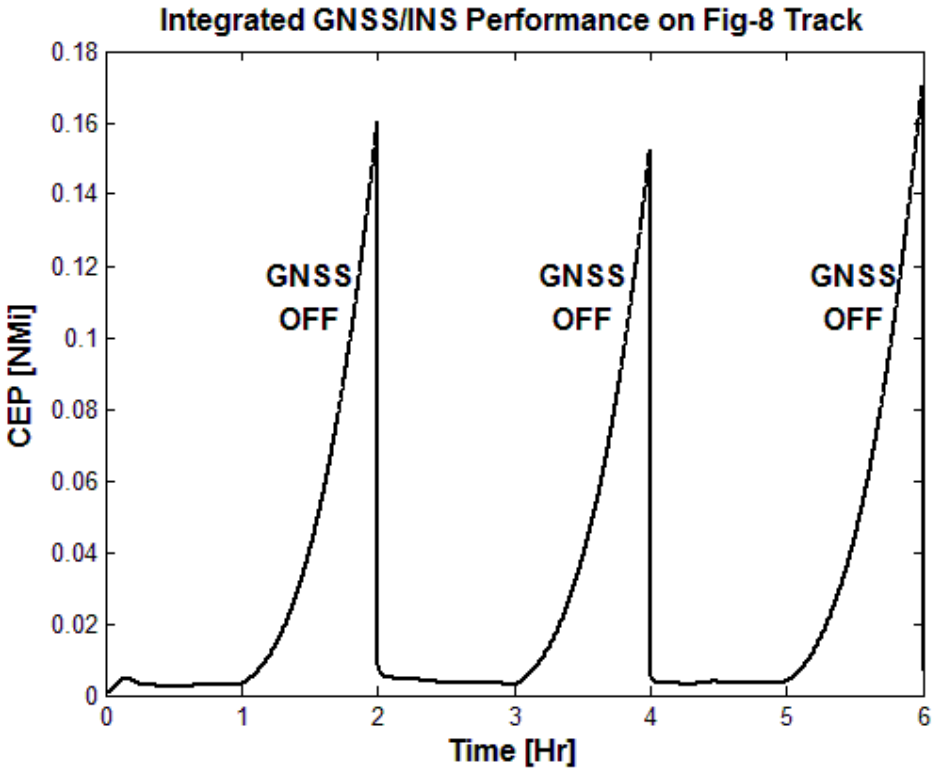

Fig 6.2: Integrated GNSS/INS Performance on Fig-8 Track

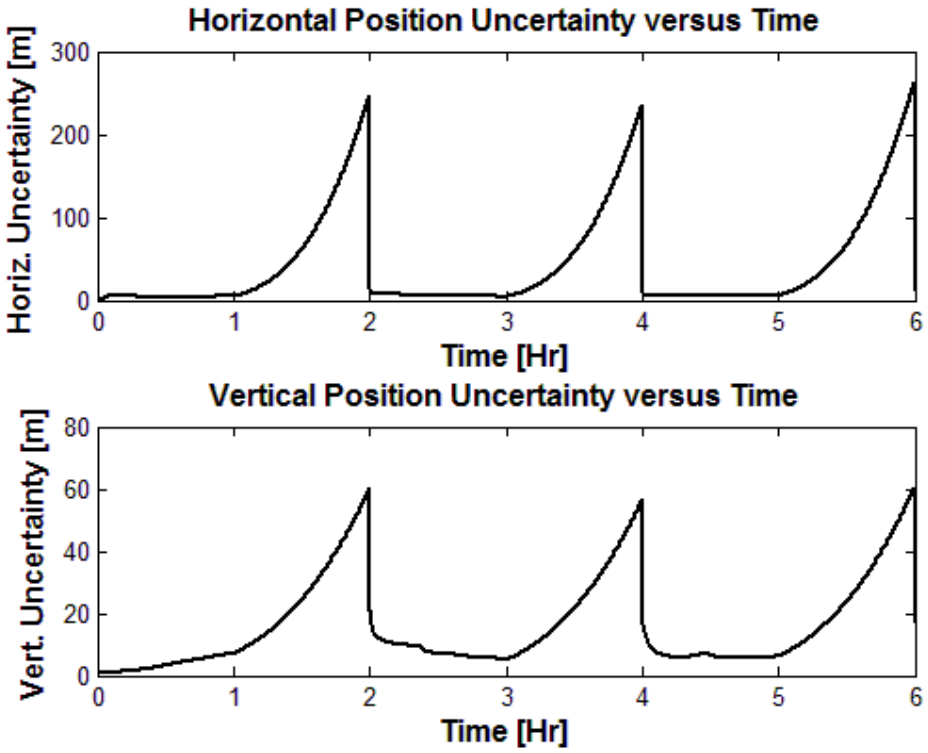

Fig 6.3: RMS Position Uncertainties

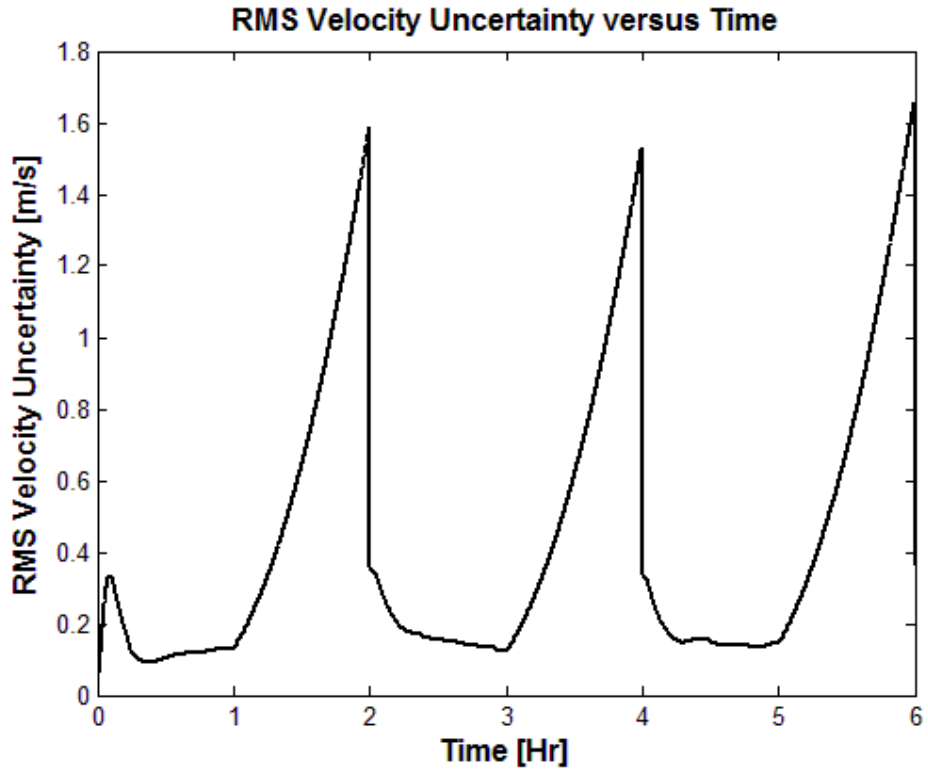

Fig 6.4: RMS Velocity Uncertainties

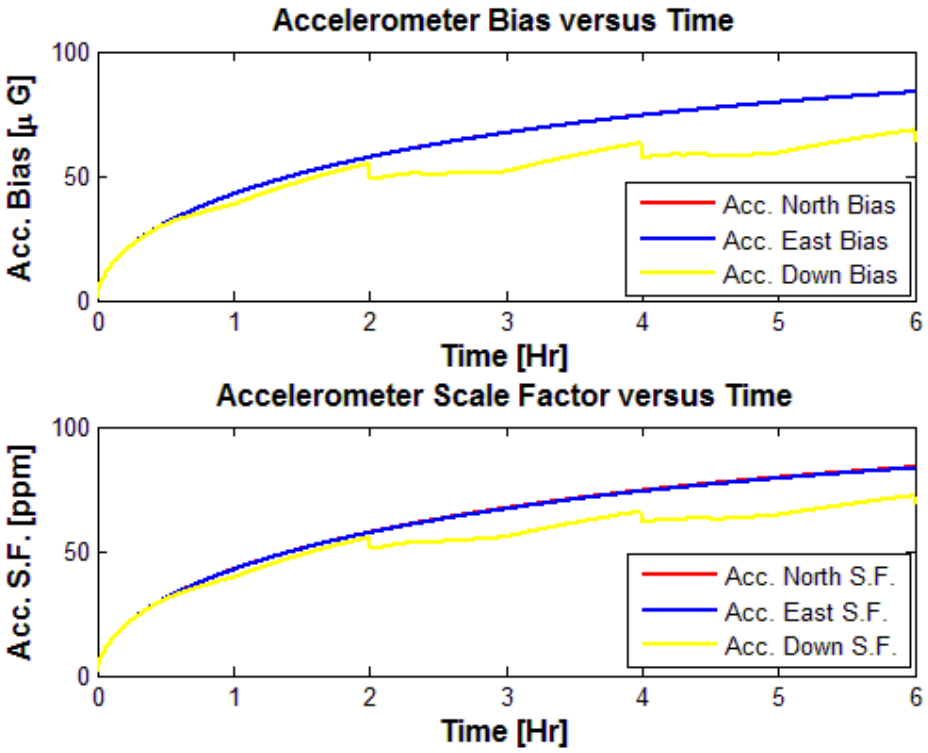

Fig 6.5: RMS Accelerometer Compensation Uncertainties

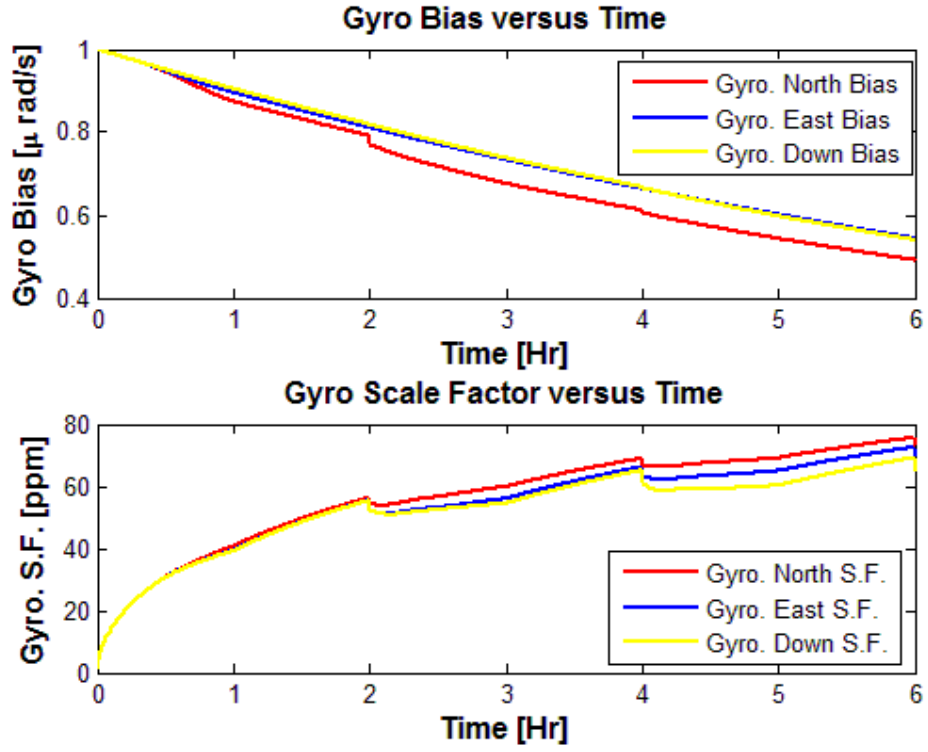

Fig 6.6: RMS Gyroscope Compensation Uncertainties

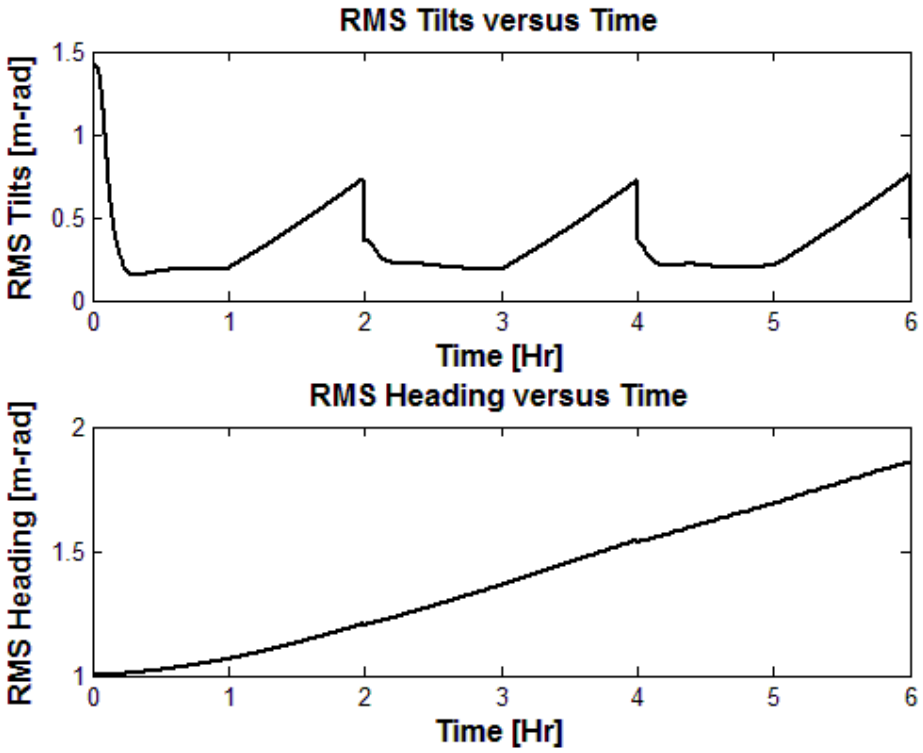

Fig 6.7: RMS Attitude Uncertainties

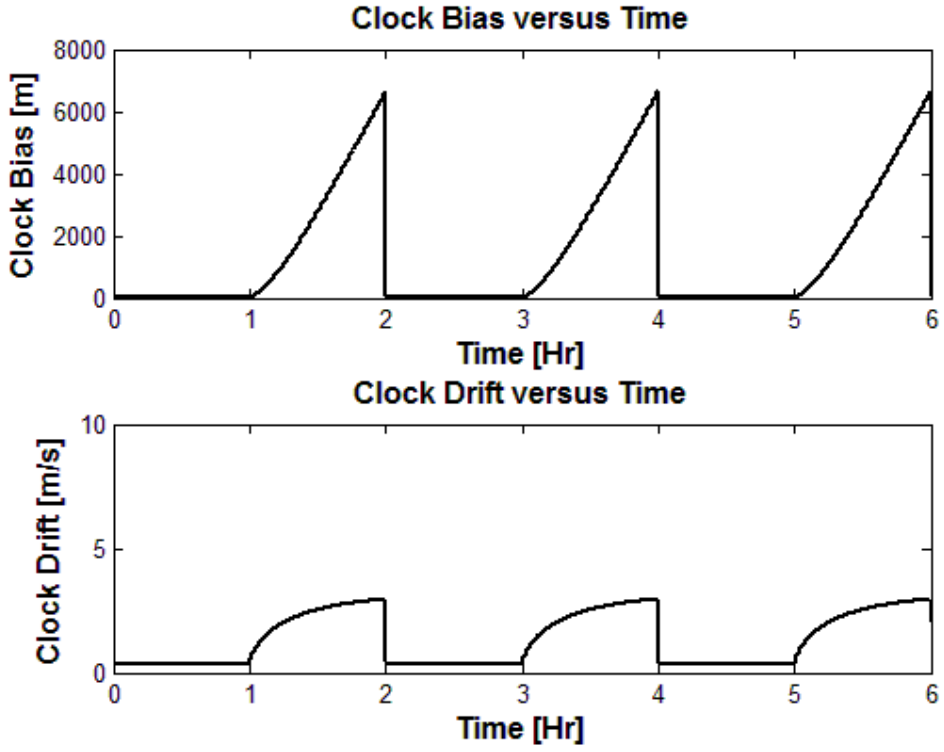

Fig 6.8: RMS Clock Parameter Uncertainties

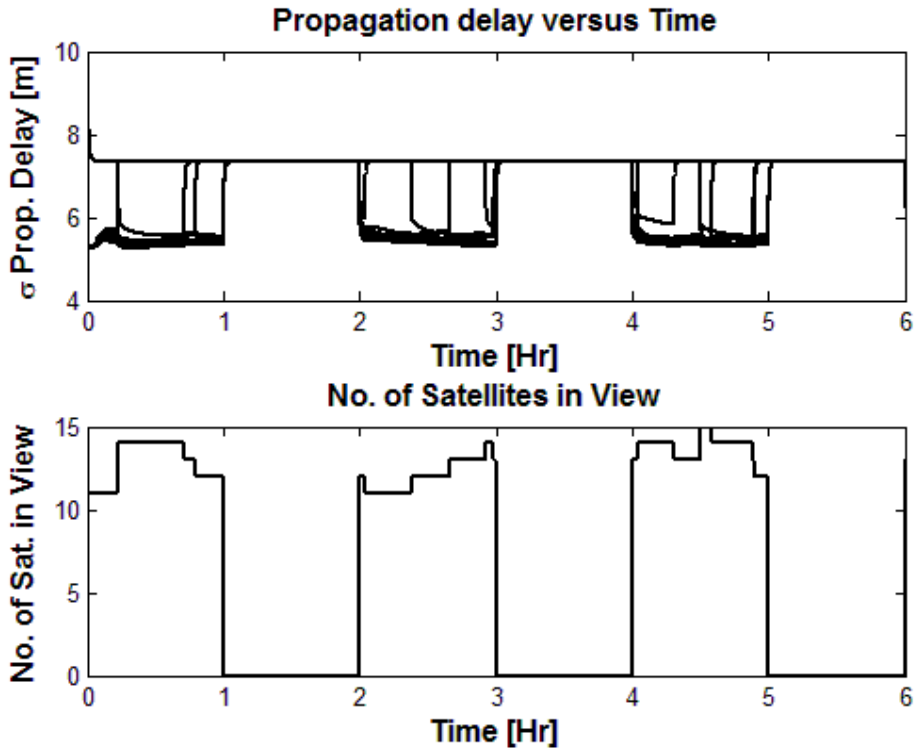

Fig 6.9: Propagation Delay and No. of Satellites in View

CEP (Circle of Equal Probability) is a measure of RMS horizontal position uncertainty. This measure is used mainly in marine navigation and its unit is Nautical Miles (NMi). Figure 6.1 shows the performance of independent INS on a figure 8 track and Figure 6.2 shows the performance of Integrated GNSS/INS system on a figure 8 track. As compared to independent INS, integrated GNSS/INS shows much better performance as is evident from the simulation results. In the integrated system, during the first hour when the GNSS signals are available, the CEP is less than 0.01 NMi which is quite good. After the first hour, the GNSS signals are neglected in the simulation. Because of the loss of GNSS signals, the uncertainties in position keeps on increasing in the integrated system which is observed by peaks in Figure 6.2. Still, the uncertainties does not rises to a very high level as compared with independent INS system of Figure 6.1. When the GNSS signals is reacquired in the integrated system, the uncertainties bounces back to its minimum level. From horizontal position uncertainty graph of Figure 6.3, it can be seen that errors in INS rises to about 250 m in one hour which is better than error accumulation rate of independent stationary INS as was observed in Figure 4.9. Hence, in an integrated system an INS can be allowed to independently navigate for some time even after the GNSS signals are lost. The integrated system does not require external aiding in the form

of altimeter to stabilize the otherwise unstable vertical errors of INS as can be seen from the vertical uncertainties of Figure 6.3 which is quite stable. The velocity uncertainties and the attitude uncertainties are also within the acceptable limits with the integrated system as observed from Figure 6.4 and Figure 6.7 respectively. Figure 6.5 and Figure 6.6 shows the effect of integration on compensation parameters (scale factors and biases) of accelerometer and gyroscope respectively. Whenever the GNSS signals are reacquired, there is a small drop in the errors of scale factors and biases in both accelerometer and gyroscope. Moreover, the compensation parameter uncertainties hardly increases when the GNSS signals are available. Apart from significant improvement in INS navigation performance due to GNSS/INS integration, the performance of GNSS receivers is also improved. The clock bias and clock drift is almost eliminated when the GNSS signals is available as can be seen from the receiver clock uncertainties of Figure 6.8. The atmospheric propagation delay of pseudoranges also becomes predictable and the corrected pseudorange can be used to provide even better estimates of position. From Figure 6.9, it can be seen that out of the 31 satellites used in simulation, only 11 to 15 satellites are in the view of GNSS receiver. From this performance analysis, it can be concluded that GNSS and INS integration using Kalman filtering have a powerful impact in the estimation of position and velocity and thus it forms a core subsystem for better navigation solution.

Chapter 7

Conclusion and Scope of Future Work

Models for INS and GNSS were successfully designed and the validity of the models were tested by performing different tests and analysis. Most of the tests were performed by taking the simulated Figure -8 track. Schuler oscillation test on INS confirms that the model for INS is valid. The performance of INS was checked under both stationary and dynamic conditions. Results obtained shows that the INS errors keeps accumulating if no external aiding is provided. Different types of GNSS filters was developed and was compared with each other. From the comparison, we can infer that DAMP3 filter is most suited for GNSS. From the study of GNSS, we also came to know that the satellite geometry also affects the positioning of the GNSS receiver. The position uncertainties of GNSS was also studied. GNSS is not as accurate as INS but its errors does not degrade over time. Whenever GNSS signals are lost, there is a decrease in accuracy of positioning of the vehicle. When GNSS and INS are integrated, the overall performance of the system is quite good and the loss of GNSS signals hardly affects the position uncertainties of the integrated system. When the GNSS signals are available the INS compensation parameters are efficiently tracked and thus with the improved initial error, an INS can be allowed to navigate for some time even when the GNSS signals are unavailable.

The design of the hardware has not been realized and the model proposed can be implemented and tested in an AUV. The system can be further fused with Doppler Velocity Log (DVL) to give even better estimate of position, velocity and attitude. DVL sensors work in the principle of Doppler Effect. DVL sends and receive sound signal reflected from the sea floor from which the velocity of the AUV can be calculated. This information can be used with the integrated GNSS/INS for better estimation of position, velocity and attitude. Further, models for Ultratightly Coupled Integration can be developed and can be used for even better estimates of navigation dynamics.

References

[1] W. Wrigley, "History of Inertial Navigation," *Navigation: Journal of the Institute of Navigation* **24**, 1-6 (1977). Baltimore

[2] L. J. Levy, "The Kalman Filter: Navigation's Integration Workhorse," *GPS World*, September 1997, pp. 65-71

[3] M. S. Grewal and A. P. Andrews, *Kalman Filtering: Theory and Practice Using MATLAB*, 3rd ed., Wiley, New York, 2008

[4] M. S. Grewal, L. R. Weill, and A. P. Andrews, *Global Positioning Systems, Inertial Navigation and Integration*, 2nd ed., Wiley, New York, 2007

[5] M. S. Grewal, A. P. Andrews, and C. G. Bartone, *Global Navigation Satellite Systems, Inertial Navigation and Integration*, 3rd ed., Wiley, New York, 2013

[6] W. S. Widnall and P. A. Grundy, *Inertial Navigation System Error Models*, Technical Report TR-03-73, Intermetrics, Cambridge, MA, May 1973

[7] A. Lawrence, *Modern Inertial Technology: Navigation, Guidance, and Control*, 2nd ed., Springer-Verlag, New York, 1993

[8] D. H. Titterton and J. L. Weston, *Strapdown Inertial Navigation Technology*, Peter Peregrinus, Stevenage, United Kingdom, 1997

[9] J. B. Y. Tsui, *Fundamentals of Global Positioning System Receivers: A Software Approach*, 2nd ed., Wiley, New York, 2004

[10] T. Fossen, *Guidance and Control of Ocean Vehicles*, John Wiley & Sons, New York, 1994

[11] J. E. Bortz, "A New Mathematical Formulation for Strapdown Inertial Navigation," *IEEE Transactions on Aerospace and Electronic Systems* **6,** 61-66 (1971)

[12] M.S. Grewal, V.D. Henderson, and R.S. Miyasako, "Application of Kalman filtering to the calibration and alignment of inertial navigation systems," *IEEE Transactions on Automatic Control* **36**, 3-13 (1991)

[13] R. Babu and J. Wang, "Ultra-tight GPS/INS/PL Integration: Kalman Filter Performance Analysis," *GNSS,* Hong Kong, 2005, pp. 8-10.